NASA Contractor Report 181983
ICASE Report No. 90–9

ICASE

TS — DEAN INTERACTIONS IN CURVED CHANNEL FLOW

Bart A. Singer
Thomas A. Zang
Gordon Erlebacher

Contract No. NAS1–18605
January 1990

Institute for Computer Applications in Science and Engineering
NASA Langley Research Center
Hampton, Virginia 23665–5225

Operated by the Universities Space Research Association

National Aeronautics and
Space Administration

Langley Research Center
Hampton, Virginia 23665-5225

TS - Dean Interactions in Curved Channel Flow

Bart A. Singer
High Technology Corporation, Hampton, VA 23666

Thomas A. Zang
NASA Langley Research Center, Hampton, VA 23665

Gordon Erlebacher *
Institute for Computer Applications in Science and Engineering
NASA Langley Research Center, Hampton, VA 23665

Abstract

A weakly nonlinear theory is developed to study the interaction of TS waves and Dean vortices in curved channel flow. The predictions obtained from the theory agree well with results obtained from direct numerical simulations of curved channel flow, especially for low amplitude disturbances. At low Reynolds numbers the wave interaction is generally stabilizing to both disturbances, though as the Reynolds number increases, many linearly unstable TS waves are further destabilized by the presence of Dean vortices.

* Research supported by the National Aeronautics and Space Administration under contract No. NAS1-18605 while resident at the Institute for Computer Applications in Science and Engineering (ICASE), NASA Langley Research Center, Hampton, VA 23665.

I. Introduction

The study of incompressible curved channel flow can illuminate some important issues dealing with laminar-turbulent transition. The streamwise curvature of the flow induces an instability resulting in longitudinal vortices (hereafter referred to as Dean vortices [1]). For the case in which the gap between the walls is small relative to the radius of curvature, Reid [2] described two approximate methods which both showed that the vortices first become unstable when the Dean number ($De = 2\mathrm{Re}\sqrt{d^*/r_i^*}$, where $\mathrm{Re} = \overline{U^*}h^*/\nu$ is the Reynolds number, $\overline{U^*}$ is the bulk velocity, d^* is the channel width, $h^* = d^*/2$ is the channel half-width, r_i^* is the inner wall radius, and ν is the kinematic viscosity) exceeds a value of about 36. These vortical structures have been found experimentally by Ligrani and Niver [3]. The linear and nonlinear properties of these axisymmetric vortices as well as their transitions into two distinct types of wavy vortices have been well documented in the direct numerical simulations and weakly nonlinear studies of Finlay, Keller, and Ferziger [4]. For more mildly curved channels than they studied, the minimum Reynolds number for instability of the Dean vortices is comparable with that for two-dimensional (2D) Tollmien-Schlichting (TS) waves. In this regime, Gibson and Cook [5] showed that oblique waves are never the dominant linear disturbance. Hence a study of the nonlinear interactions between 2D TS waves and the streamwise oriented Dean vortices can be meaningfully conducted.

Daudpota, Hall and Zang [6] (hereafter referred to as DHZ) developed a weakly nonlinear interaction theory to study the interaction of Dean vortices and TS waves in curved channels. They employed a multiple scale version of the Stuart [7] and Watson [8] approach to derive two coupled Landau equations for the perturbation amplitudes of Dean vortices and TS waves. A comparison of their theory's predictions with the results of direct numerical simulation [9] suggests that their results are in error with respect to the influence of the TS wave on the Dean vortex. The resolution of this discrepancy is the major motivation for undertaking this work. In section II. we present a slightly different formulation of a weakly nonlinear interaction theory and describe how the resulting equations are solved. The current approach is based on the work by Herbert [10, 11]. We compare some aspects of this approach with that used by DHZ. In section III. we report some results of the interaction theory while in section IV. we compare specific cases with results of direct numerical simulation. Finally in section V. we draw conclusions.

II. Mathematical Formulation

A. *The Basic Equations*

The incompressible Navier-Stokes equations in cylindrical coordinates (r^*, θ, z^*) are written as:

$$\frac{1}{r^*}\frac{\partial (r^* U_r{}^*)}{\partial r^*} + \frac{1}{r^*}\frac{\partial U_\theta{}^*}{\partial \theta} + \frac{\partial U_z{}^*}{\partial z^*} = 0 \tag{1}$$

$$\frac{\partial U_r{}^*}{\partial t^*} + \left(\vec{V}^* \cdot \vec{\nabla}^*\right) U_r{}^* - \frac{1}{r^*} U_\theta{}^{*2} = -\frac{1}{\rho^*}\frac{\partial P^*}{\partial r^*} + \nu^* \left(\nabla^{*2} U_r{}^* - \frac{U_r{}^*}{r^{*2}} - \frac{2}{r^{*2}}\frac{\partial U_\theta{}^*}{\partial \theta}\right) \tag{2}$$

$$\frac{\partial U_\theta{}^*}{\partial t^*} + \left(\vec{V}^* \cdot \vec{\nabla}^*\right) U_\theta{}^* + \frac{U_\theta{}^* U_r{}^*}{r^*} = -\frac{1}{r^* \rho^*}\frac{\partial P^*}{\partial \theta} + \nu^* \left(\nabla^{*2} U_\theta{}^* - \frac{U_3{}^*}{r^{*2}} + \frac{2}{r^{*2}}\frac{\partial U_r{}^*}{\partial \theta}\right) \tag{3}$$

$$\frac{\partial U_z{}^*}{\partial t^*} + \left(\vec{V}^* \cdot \vec{\nabla}^*\right) U_z{}^* = -\frac{1}{\rho^*}\frac{\partial P^*}{\partial z^*} + \nu^* \nabla^{*2} U_z{}^* \tag{4}$$

where:

$$\vec{V}^* \cdot \vec{\nabla}^* = U_r{}^* \frac{\partial}{\partial r^*} + \frac{U_\theta{}^*}{r^*}\frac{\partial}{\partial \theta} + U_z{}^* \frac{\partial}{\partial z^*} \tag{5}$$

$$\nabla^{*2} = \frac{1}{r^*}\frac{\partial}{\partial r^*}\left(r^* \frac{\partial}{\partial r^*}\right) + \frac{1}{r^{*2}}\frac{\partial^2}{\partial \theta^2} + \frac{\partial^2}{\partial z^{*2}} \tag{6}$$

and ρ^* and ν^* represent the constant density and kinematic viscosity respectively. The asterisks indicate dimensional quantities. The geometry of the problem of azimuthal flow between infinite concentric walls of outer radius r_o^* and inner radius r_i^* is illustrated in Figure 1. The wall boundary conditions require that:

$$U_r{}^* = U_\theta{}^* = U_z{}^* = 0, \qquad \text{at } r^* = r_i^*,\ r_o^*. \tag{7}$$

A solution to the equations gives $(U_r{}^*, U_\theta{}^*, U_z{}^*, P^*)$ as:

$$\begin{pmatrix} U_r{}^* \\ U_\theta{}^* \\ U_z{}^* \\ P^* \end{pmatrix} = \begin{pmatrix} 0 \\ \overline{U^*} f(r^*) \\ 0 \\ \theta \rho^* \overline{U^*}^2 \int f(r)^2/r dr \end{pmatrix}. \tag{8}$$

Here $\overline{U^*}$ is the bulk velocity and

$$f(r^*) = D^* \left(r^* \log r^* + C^* r^* + E^*/r^*\right)$$

where:

$$C^* = \left(r_i^{*2} \log r_i^* - r_o^{*2} \log r_o^*\right) / \left(r_o^{*2} - r_i^{*2}\right) \tag{9}$$

$$E^* = -(r_i^* r_o^*)^2 / (r_o^{*2} - r_i^{*2}) \log \eta \tag{10}$$

$$D^* = -2/(r_c^* + E^*/h^* \log \eta). \tag{11}$$

The quantity $r_c^* = (r_o^* + r_i^*)/2$ is the centerline radius and the ratio $\eta = r_i^*/r_o^*$ describes the channel curvature.

We nondimensionalize all spatial coordinates with the channel half-width, velocities with the bulk velocity, and pressure with $\rho^* \overline{U^*}^2$. The temporal scale is $h^*/\overline{U^*}$. The Reynolds number is defined as

$$\mathrm{Re} = \overline{U^*} h^* / \nu^*.$$

The nondimensional equations are easily obtained from the dimensional ones by replacing all starred quantities with their corresponding nondimensional unstarred ones and noting that $\rho = 1$, $h = 1$, and $\nu = 1/\mathrm{Re}$. The expression $1 - \eta$ appears often below and is denoted by λ. When $\lambda = \lambda_c = 2.179 \times 10^{-5}$ the minimum Reynolds number for instability of TS waves is the same as that for Dean vortices (see Gibson and Cook[5]).

We follow closely the perturbation method introduced by Herbert [10, 11], extending it to the case of interacting disturbances. The steady solution is perturbed such that

$$\begin{pmatrix} U_r \\ U_\theta \\ U_z \\ P \end{pmatrix} = \begin{pmatrix} u_r \\ f(r) + u_\theta \\ u_z \\ \theta \int f^2/r dr + p \end{pmatrix} \tag{12}$$

where u_r, u_θ, u_z, and p are perturbation quantities. Substituting the perturbations into the nondimensionalized Navier-Stokes equations, subtracting the steady flow component, and rearranging gives:

$$\frac{1}{r}\frac{\partial (r u_r)}{\partial r} + \frac{1}{r}\frac{\partial u_\theta}{\partial \theta} + \frac{\partial u_z}{\partial z} = 0 \tag{13}$$

$$\frac{\partial u_r}{\partial t} + \frac{\partial p}{\partial r} - \frac{1}{r} 2 f u_\theta + \frac{f}{r}\frac{\partial u_r}{\partial \theta} - \frac{1}{\mathrm{Re}}\left(\nabla^2 u_r - \frac{u_r}{r^2} - \frac{2}{r^2}\frac{\partial u_\theta}{\partial \theta}\right) = -\left(\vec{V}\cdot\vec{\nabla}\right) u_r + \frac{1}{r} u_\theta^2 \tag{14}$$

$$\frac{\partial u_\theta}{\partial t} + \frac{1}{r}\frac{\partial p}{\partial \theta} + \frac{f u_r}{r} + \frac{f}{r}\frac{\partial}{\partial \theta} u_\theta + \left(\vec{V}\cdot\vec{\nabla}\right) f - \frac{1}{\mathrm{Re}}\left(\nabla^2 u_\theta - \frac{u_\theta}{r^2} + \frac{2}{r^2}\frac{\partial u_r}{\partial \theta}\right) = -\left(\vec{V}\cdot\vec{\nabla}\right) u_\theta - \frac{u_\theta u_r}{r} \tag{15}$$

$$\frac{\partial u_z}{\partial t} + \frac{\partial p}{\partial z} + \frac{f}{r}\frac{\partial u_z}{\partial \theta} - \frac{1}{\mathrm{Re}}\nabla^2 u_z = -\left(\vec{V}\cdot\vec{\nabla}\right) u_z \tag{16}$$

where:

$$\vec{V}\cdot\vec{\nabla} = u_r\frac{\partial}{\partial r} + \frac{u_\theta}{r}\frac{\partial}{\partial \theta} + u_z\frac{\partial}{\partial z} \tag{17}$$

$$\nabla^2 = \frac{1}{r}\frac{\partial}{\partial r}\left(r\frac{\partial}{\partial r}\right) + \frac{1}{r^2}\frac{\partial^2}{\partial \theta^2} + \frac{\partial^2}{\partial z^2} \tag{18}$$

The entire flow is assumed to be periodic in the azimuthal (streamwise) and axial (spanwise) directions; the solution evolves in time. In addition the total pressure gradient is kept constant.

B. Fourier Expansions

The linearized disturbance equations are obtained by setting the right hand sides of Equations 13-16 equal to zero. A solution to the equations for a 2D TS wave can be written as:

$$\begin{pmatrix} u_r \\ u_\theta \\ u_z \\ p \end{pmatrix} = \begin{pmatrix} \tilde{u_r}^{1,0}(r,t) \\ \tilde{u_\theta}^{1,0}(r,t) \\ 0 \\ \tilde{p}^{1,0}(r,t) \end{pmatrix} \exp i(\alpha\theta - \gamma(t)). \tag{19}$$

Here α is real and represents the azimuthal wavenumber while $\gamma(t) = g_0 t$ is a real function defining the phase. Any growth or decay of the TS wave is expressed in terms of an amplitude parameter such that:

$$\begin{pmatrix} \tilde{u_r}^{1,0}(r,t) \\ \tilde{u_\theta}^{1,0}(r,t) \\ 0 \\ \tilde{p}^{1,0}(r,t) \end{pmatrix} = A(t) \begin{pmatrix} \hat{u_r}^{1,0,0,0}(r) \\ \hat{u_\theta}^{1,0,0,0}(r) \\ 0 \\ \hat{p}^{1,0,0,0}(r) \end{pmatrix} \tag{20}$$

where

$$\frac{dA}{dt} = a_{0,0} A \tag{21}$$

and $a_{0,0}$ is the linear growth rate. The apparently superfluous superscripts and subscripts are included here for consistency with the notation used later. A convenient normalization for this problem is

$$|\tilde{u_r}^{1,0}(r_c,t)| = A(t) \tag{22}$$

where r_c is the channel centerline. We take

$$\hat{u_r}^{1,0,0,0}(r_c) = 1, \tag{23}$$

thus fixing the amplitude and phase of the TS wave.

In a similar manner, one can write the solution for the primary Dean vortex mode as:

$$\begin{pmatrix} u_r \\ u_\theta \\ u_z \\ p \end{pmatrix} = \begin{pmatrix} \tilde{u_r}^{0,1}(r,t) \\ \tilde{u_\theta}^{0,1}(r,t) \\ \tilde{u_z}^{0,1}(r,t) \\ \tilde{p}^{0,1}(r,t) \end{pmatrix} \exp i(\beta z - \zeta(t)), \tag{24}$$

where β is the real axial wavenumber and $\zeta(t) = h_0 t = 0$ indicates that the linear Dean disturbance is steady. We also write

$$\begin{pmatrix} \tilde{u_r}^{0,1}(r,t) \\ \tilde{u_\theta}^{0,1}(r,t) \\ \tilde{u_z}^{0,1}(r,t) \\ \tilde{p}^{0,1}(r,t) \end{pmatrix} = B(t) \begin{pmatrix} \hat{u_r}^{0,0,1,0}(r) \\ \hat{u_\theta}^{0,0,1,0}(r) \\ \hat{u_z}^{0,0,1,0}(r) \\ \hat{p}^{0,0,1,0}(r) \end{pmatrix} \tag{25}$$

where

$$\frac{dB}{dt} = b_{0,0}B. \tag{26}$$

The normalization is chosen such that:

$$|\tilde{u_r}^{0,1}(r_c,t)| = B(t), \tag{27}$$

or in this case,

$$\hat{u_r}^{0,0,1,0}(r_c) = 1. \tag{28}$$

It is conceivable that a particularly inauspicious choice of the parameters Re , λ, and wavenumbers might lead to $\hat{u_r}^{1,0,0,0}(r_c) = 0$ or $\hat{u_r}^{0,0,1,0}(r_c) = 0$ and hence the normalization used in either Equation 22 or 27 could fail. Such an event would lead to overflow errors in the numerical procedure and an alternative normalization could be used. Herbert [11] discusses integral normalizations which are more robust but somewhat more complicated to implement. In practice we have never experienced any problems with the normalizations in Equations 22 and 27. We attribute this to the fact that the amplitudes of the radial velocities of the dominant TS waves and Dean vortices do not have local minima near the channel center.

When the nonlinear terms (the right hand sides of Equations 13-16) are included, the disturbances can interact with themselves, the mean flow, each other and all their relevant complex conjugates. This results in the generation of harmonics, mean flow distortions, and various corrections to the fundamental disturbances. Hence it is natural to expand the perturbation variables in a double Fourier series:

$$\begin{pmatrix} u_r \\ u_\theta \\ u_z \\ p \end{pmatrix} = \sum_{n=-\infty}^{\infty} \sum_{l=-\infty}^{\infty} \begin{pmatrix} \tilde{u_r}^{n,l}(r,t) \\ \tilde{u_\theta}^{n,l}(r,t) \\ \tilde{u_z}^{n,l}(r,t) \\ \tilde{p}^{n,l}(r,t) \end{pmatrix} \exp in(\alpha\theta - \gamma(t)) \exp il(\beta z - \zeta(t)). \tag{29}$$

C. Amplitude Expansion

The system of nonlinear partial differential equations obtained by substituting Equation 29 into Equations 13– 16 are coupled and difficult to solve efficiently. We seek a solution by expanding in the amplitude parameters $A(t)$ and $B(t)$ about the linear solutions given by Equations 19 and 24. The solutions will reflect the deviations from linear behavior for finite, but sufficiently small amplitudes A and B. In this context, all harmonics of the primary disturbances are considered to be forced. Since the linear TS and Dean solutions are $O(A)$ and $O(B)$ respectively, their first harmonics and cross terms will be $O(A^2)$, $O(B^2)$, and $O(AB)$. Higher order harmonics and cross terms will be $O(A^nB^l)$, hence it is reasonable to let:

$$\begin{pmatrix} \tilde{u_r}^{n,l}(r,t) \\ \tilde{u_\theta}^{n,l}(r,t) \\ \tilde{u_z}^{n,l}(r,t) \\ \tilde{p}^{n,l}(r,t) \end{pmatrix} = A^{|n|}B^{|l|} \begin{pmatrix} \tilde{\tilde{u_r}}^{n,l}(r,t) \\ \tilde{\tilde{u_\theta}}^{n,l}(r,t) \\ \tilde{\tilde{u_z}}^{n,l}(r,t) \\ \tilde{\tilde{p}}^{n,l}(r,t) \end{pmatrix} \tag{30}$$

where all double tilde terms are $O(1)$ except for those with $n = l = 0$. Heuristically, one can see that the exception with the $n = l = 0$ term comes about from the fact that the lowest order mean flow distortions are generated from the product of either TS or Dean fundamental disturbances with their respective complex conjugates. Since the fundamental disturbances are $O(A)$ and $O(B)$, the product terms which generate $n = l = 0$ are $O(A^2)$ and $O(B^2)$ respectively. Substitution of the representation in Equation 30 into Equation 29 gives:

$$\begin{pmatrix} u_r \\ u_\theta \\ u_z \\ p \end{pmatrix} = \sum_{n=-\infty}^{\infty} \sum_{l=-\infty}^{\infty} \begin{pmatrix} \tilde{\tilde{u}}_r^{\,n,l}(r,t) \\ \tilde{\tilde{u}}_\theta^{\,n,l}(r,t) \\ \tilde{\tilde{u}}_z^{\,n,l}(r,t) \\ \tilde{\tilde{p}}^{n,l}(r,t) \end{pmatrix} A^{|n|}(t) B^{|l|}(t) \exp in(\alpha\theta - \gamma(t)) \exp il(\beta z - \zeta(t)). \quad (31)$$

Since we seek solutions which are small deviations from the linear behavior, we now expand the double tilde representations in sums which are the products of ascending powers of the amplitude functions with coefficients which are strictly functions of the radial coordinate. In the limit as $A \to 0$ and $B \to 0$, the solutions tend towards the linear results. Because of the invariance of the original equations and boundary conditions with respect to arbitrary translation in the streamwise and spanwise directions and the assumption of periodicity of the solutions in these directions, only even powers of A and B are needed [12]. Hence,

$$\begin{pmatrix} \tilde{\tilde{u}}_r^{\,n,l}(r,t) \\ \tilde{\tilde{u}}_\theta^{\,n,l}(r,t) \\ \tilde{\tilde{u}}_z^{\,n,l}(r,t) \\ \tilde{\tilde{p}}^{n,l}(r,t) \end{pmatrix} = \sum_{m=0}^{\infty} \sum_{k=0}^{\infty} \begin{pmatrix} \hat{u}_r^{\,n,m,l,k}(r) \\ \hat{u}_\theta^{\,n,m,l,k}(r) \\ \hat{u}_z^{\,n,m,l,k}(r) \\ \hat{p}^{n,m,l,k}(r) \end{pmatrix} A^{2m}(t) B^{2k}(t). \quad (32)$$

By substitution into Equation 31 one obtains the full representation of the perturbation variables:

$$\begin{pmatrix} u_r \\ u_\theta \\ u_z \\ p \end{pmatrix} = \sum_{n=-\infty}^{\infty} \sum_{m=0}^{\infty} \sum_{l=-\infty}^{\infty} \sum_{k=0}^{\infty} \begin{pmatrix} \hat{u}_r^{\,n,m,l,k}(r) \\ \hat{u}_\theta^{\,n,m,l,k}(r) \\ \hat{u}_z^{\,n,m,l,k}(r) \\ \hat{p}^{n,m,l,k}(r) \end{pmatrix} A^{2m+|n|}(t) B^{2k+|l|}(t)$$
$$\exp in(\alpha\theta - \gamma(t)) \exp il(\beta z - \zeta(t)). \quad (33)$$

In order that the wall boundary conditions be satisfied at all orders of approximation, we require:

$$\begin{pmatrix} \hat{u}_r^{\,n,m,l,k}(r) \\ \hat{u}_\theta^{\,n,m,l,k}(r) \\ \hat{u}_z^{\,n,m,l,k}(r) \end{pmatrix} = \begin{pmatrix} 0 \\ 0 \\ 0 \end{pmatrix} \qquad \text{at } r = r_i,\ r_o \quad (34)$$

for all combinations of n, m, l, and k.

The time derivatives $\dot{A}/A$, $\dot{B}/B$, $\dot{\gamma}$, and $\dot{\zeta}$ are also expanded in terms of A^2 and B^2 such that:

$$\frac{\dot{A}}{A} = \sum_{m=0}^{\infty} \sum_{k=0}^{\infty} a_{m,k} A^{2m} B^{2k} \quad (35)$$

$$\frac{\dot{B}}{B} = \sum_{m=0}^{\infty}\sum_{k=0}^{\infty} b_{m,k} A^{2m} B^{2k} \tag{36}$$

$$\dot{\gamma} = \sum_{m=0}^{\infty}\sum_{k=0}^{\infty} g_{m,k} A^{2m} B^{2k} \tag{37}$$

$$\dot{\zeta} = \sum_{m=0}^{\infty}\sum_{k=0}^{\infty} h_{m,k} A^{2m} B^{2k} \tag{38}$$

Equations 35 and 36 are the coupled Landau equations which describe the growth of the disturbances. The purpose of the remainder of this section is to determine the Landau coefficients $a_{m,k}$ and $b_{m,k}$.

D. Solution Method

The solution expansions in Equations 31–38 are substituted into the perturbation equations 13–16. All terms with common exponential factors are grouped together. The simplest nonlinear theory is obtained by considering only those terms with Fourier exponents limited by:

$$-2 \leq n, l \leq 2.$$

With this restriction, it is only appropriate to consider terms in the amplitude expansions (Equation 32) with $m = 0, 1$ and $k = 0, 1$. Larger values of m or k give higher order contributions which should not be considered at this degree of truncation. In each group with common exponential factors, all terms with common powers of A and B are collected. This tedious process of expanding the solutions, substituting into the equations and collecting terms with common factors of exponentials and amplitude parameters is done automatically using the symbolic manipulator Macsyma. The case $n = m = l = k = 0$ just represents the basic flow which has already been subtracted out. A sequence of 12 systems of equations remains. Each system contains four equations and four unknown expansion coefficients which are functions of r. A description of each of the systems is summarized in Table 1. The equation system number indicates the order in which we chose to solve the equations. To ensure that all information needed to solve any system has already been computed, all systems of lower order in the amplitude parameters should be solved before those of higher order.

The first two equation systems are eigenproblems of the form:

$$\mathbf{L}_{n,l}\hat{\mathbf{q}}_{n,0,l,0} = +\left(n\left(a_{0,0} - ig_{0,0}\right) + l\left(b_{0,0} - ih_{0,0}\right)\right)\mathbf{M}\hat{\mathbf{q}}_{n,0,l,0} \tag{39}$$

where:

$$\hat{\mathbf{q}}_{n,m,l,k} = \begin{pmatrix} \hat{u_r}^{n,m,l,k}(r) \\ \hat{u_\theta}^{n,m,l,k}(r) \\ \hat{u_z}^{n,m,l,k}(r) \\ \hat{p}^{n,m,l,k}(r) \end{pmatrix} \tag{40}$$

Eq. Sys. No.	Order	n	m	l	k	Description
1	A	1	0	0	0	Linear TS wave
2	B	0	0	1	0	Linear Dean vortex
3	A^2	0	1	0	0	Mean flow distortion from TS
4	B^2	0	0	0	1	Mean flow distortion from Dean
5	A^2	2	0	0	0	TS harmonic
6	B^2	0	0	2	0	Dean harmonic
7	AB	1	0	1	0	TS – Dean cross harmonic
8	AB	1	0	-1	0	TS – Dean cross harmonic
9	A^3	1	1	0	0	Self-correction to TS
10	B^3	0	0	1	1	Self-correction to Dean
11	AB^2	1	0	0	1	Dean correction to TS
12	A^2B	0	1	1	0	TS correction to Dean

Table 1: Summary of equation systems

and

$$\mathbf{M} = \begin{pmatrix} -1 & 0 & 0 & 0 \\ 0 & -1 & 0 & 0 \\ 0 & 0 & -1 & 0 \\ 0 & 0 & 0 & 0 \end{pmatrix} \tag{41}$$

For the eigenproblems, the indices n and l may only have the values 0 and 1 with the constraint $n + l = 1$. The elements of the operator $\mathbf{L}_{n,l}$ are given in Appendix A. The solution of the eigenproblem determines the eigenvalues (we consider here only the least stable ones), $a_{0,0} + ig_{0,0}$ and $b_{0,0} + ih_{0,0}$. The eigenvectors $\hat{\mathbf{q}}_{1,0,0,0}(r)$ and $\hat{\mathbf{q}}_{0,0,1,0}(r)$ are known to within a constant factor. The normalizations in Equations 23 and 28 are used for the two eigenvectors. The real parts of the eigenvalues are the zeroth order Landau coefficients.

Equation systems 3 and 4 represent the mean flow distortion caused by the TS and Dean disturbances respectively. For this case, $n = l = 0$ and the operator $\mathbf{L}_{n,l}$ can be greatly simplified. Here we consider only the case where either m or k equals 1, while the other equals 0. Earlier we specified that the mean pressure gradient is constant, $\hat{p}^{0,1,0,0} = \hat{p}^{0,0,0,1} = 0$. Analysis indicates that $\hat{u_r}^{0,1,0,0} = \hat{u_r}^{0,0,0,1} = \hat{u_z}^{0,1,0,0} = \hat{u_z}^{0,0,0,1} = 0$. The remaining equation can be written as:

$$\begin{aligned} (2ma_{0,0} + 2kb_{0,0} + \tfrac{1}{r^2\mathrm{Re}})\hat{u_\theta}^{0,m,0,k} - \tfrac{1}{r\mathrm{Re}}\tfrac{d}{dr}\hat{u_\theta}^{0,m,0,k} - \tfrac{1}{\mathrm{Re}}\tfrac{d^2}{dr^2}\hat{u_\theta}^{0,m,0,k} = \\ ik\beta(\hat{u_\theta}^{0,0,-1,0}\hat{u_z}^{0,0,1,0} - \hat{u_\theta}^{0,0,1,0}\hat{u_z}^{0,0,-1,0}) \\ -(\hat{u_\theta}^{-m,0,-k,0}\hat{u_r}^{m,0,k,0} + \hat{u_\theta}^{m,0,k,0}\hat{u_r}^{-m,0,-k,0})/r \\ -(\tfrac{d}{dr}(\hat{u_\theta}^{-m,0,-k,0})\hat{u_r}^{m,0,k,0} + \tfrac{d}{dr}(\hat{u_\theta}^{m,0,k,0})\hat{u_r}^{-m,0,-k,0}). \end{aligned} \tag{42}$$

An interesting restriction to the theory results from Equation 42. Consider the associated homogeneous problem:

$$(2ma_{0,0} + 2kb_{0,0} + \frac{1}{r^2\mathrm{Re}})\phi - \frac{1}{r\mathrm{Re}}\frac{d\phi}{dr} - \frac{1}{\mathrm{Re}}\frac{d^2\phi}{dr^2} = 0$$

with boundary conditions:

$$\phi = 0 \qquad \text{at } r = r_i, r_o.$$

Apply the transformation:

$$r^2 = \xi^2 / \left(-(2ma_{0,0} + 2kb_{0,0})\mathrm{Re}\right)$$

to the homogeneous problem and divide by $(2ma_{0,0} + 2kb_{0,0})$ to obtain:

$$(1 - \frac{1}{\xi^2})\phi + \frac{1}{\xi}\frac{d\phi}{d\xi} + \frac{d^2\phi}{d\xi^2} = 0 \tag{43}$$

with

$$\phi = 0 \qquad \text{at } \xi = \xi_i, \xi_o$$

where

$$\xi_i^2 = r_i^2 / \left(-(2ma_{0,0} + 2kb_{0,0})\mathrm{Re}\right)$$
$$\xi_o^2 = r_o^2 / \left(-(2ma_{0,0} + 2kb_{0,0})\mathrm{Re}\right)$$

Equation 43 is the Bessel equation of order 1. If the points ξ_i and ξ_o correspond to zeros of the appropriate Bessel function, then this free eigenmode can contribute an arbitrarily large component to the solution of the forced problem. Moreover, a numerically ill-conditioned system arises whenever ξ_i and ξ_o are both in the neighborhood of zeros of the Bessel function. A sure way to prevent this problem is to require both $a_{0,0}$ and $b_{0,0}$ to be non-negative. This essentially restricts the application of the theory to those regimes in Reynolds number – wavenumber space where both the TS and Dean disturbances are unstable. In this regime, solving for $\hat{u_\theta}^{0,1,0,0}$ and $\hat{u_\theta}^{0,0,0,1}$ is straightforward.

The equation systems 5–12 are all of the form:

$$\left(\mathbf{L}_{n,l} - (2ma_{0,0} + |n|a_{0,0} - ing_{0,0} + 2kb_{0,0} + |l|b_{0,0} - ilh_{0,0})\,\mathbf{M}\right)\hat{\mathbf{q}}_{n,m,l,k} = \mathbf{R}_s, \tag{44}$$

where $\mathbf{R}_s$ is the right hand side vector of the s equation system. The right hand side vectors consist of nonlinear combinations of the solutions obtained at lower order. The elements of the right hand side vectors are given explicitly in the Appendix B. Some important considerations in solving the equations are given below. (Many of these issues are addressed in detail by Herbert [11] for the case of a single 2D TS wave in a straight channel.)

With the restriction that $a_{0,0}$ and $b_{0,0}$ be non-negative, the homogeneous problems associated with Equation 44 are unlikely to have free modes. The occurrence of any free modes for Dean harmonics would require that $(2k + l)b_{0,0}$ be an eigenvalue for the homogeneous problem with wavenumber $l\beta$. (Note that $h_{0,0} = 0$.) Such an unlikely coincidence would lead to obviously nonsensical results of the numerical solution. TS harmonics and crossed TS-Dean harmonics would be even less likely to have free modes because both real and imaginary parts of the eigenvalue would need to match.

Equation systems 5–8 for the various harmonics require numerically solving a sequence of linear ordinary differential equation systems. In the case of Dean disturbances, it is possible that the harmonic of an unstable mode is also in the unstable regime. When this happens, it violates the assumption that all of the higher harmonics are forced by the primary disturbances. While numerical results can be obtained for such cases, the results are meaningless since the harmonic can grow on its own and is not simply forced by the fundamental.

Equation systems 9–12 define the corrections to the fundamental TS and Dean disturbances and allow us to calculate the Landau coefficients $a_{1,0}$, $b_{0,1}$, $a_{0,1}$, and $b_{1,0}$ respectively. It is in the solution of these terms that the method developed by Herbert [10, 11] differs significantly from the standard Stuart [7] and Watson [8] approach.

The right hand side vectors $\mathbf{R}_s$ for $s = 9$–12 can be rewritten as:

$$\mathbf{R}_s = \mathbf{R}'_s + \kappa_s \mathbf{M} \hat{\mathbf{q}}_{n,0,l,0} \tag{45}$$

where:

$$\begin{aligned} \kappa_9 &= a_{1,0} - i g_{1,0} \\ \kappa_{10} &= b_{0,1} - i h_{0,1} \\ \kappa_{11} &= a_{0,1} - i g_{0,1} \\ \kappa_{12} &= b_{1,0} - i h_{1,0}. \end{aligned}$$

The correspondence between the index s and the indices n, m, l, and k is given in Table 1. Note that these equations have either $n = 1$, $l = 0$, or $n = 0$, $l = 1$. No other combinations of n and l appear. The solution vectors $\hat{\mathbf{q}}_{n,m,l,k}$ for these equation systems are the sums of particular solution vectors, hence it is useful to write:

$$\hat{\mathbf{q}}_{n,m,l,k}(r) = \kappa_s \chi^0_{n,m,l,k}(r) + \chi^1_{n,m,l,k}(r) \tag{46}$$

where:

$$\chi^0_{n,m,l,k}(r_i) = \chi^0_{n,m,l,k}(r_o) = \chi^1_{n,m,l,k}(r_i) = \chi^1_{n,m,l,k}(r_o) = 0. \tag{47}$$

Substitution of Equations 45 and 46 into 44 leads to:

$$\left(\mathbf{L}_{n,l} - \left(2ma_{0,0} + n(a_{0,0} - i g_{0,0}) + 2kb_{0,0} + l(b_{0,0} - i h_{0,0})\right)\mathbf{M}\right) \kappa_s \chi^0_{n,m,l,k} = \kappa_s \mathbf{M} \hat{\mathbf{q}}_{n,0,l,0} \tag{48}$$

$$\left(\mathbf{L}_{n,l} - \left(2ma_{0,0} + n(a_{0,0} - i g_{0,0}) + 2kb_{0,0} + l(b_{0,0} - i h_{0,0})\right)\mathbf{M}\right) \chi^1_{n,m,l,k} = \mathbf{R}'_s. \tag{49}$$

Recognizing that

$$\left(\mathbf{L}_{n,l} - \left(n(a_{0,0} - i g_{0,0}) + l(b_{0,0} - i h_{0,0})\right)\mathbf{M}\right) \hat{\mathbf{q}}_{n,0,l,0} = 0 \tag{50}$$

when $n = 1$, $l = 0$ or $n = 0$, $l = 1$, one finds by inspection of Equation 48:

$$-\left(2ma_{0,0} + 2kb_{0,0}\right) \chi^0_{n,m,l,k} = \hat{\mathbf{q}}_{n,0,l,0} \tag{51}$$

or

$$\chi^0_{n,m,l,k} = -\hat{\mathbf{q}}_{n,0,l,0} / \left(2ma_{0,0} + 2kb_{0,0}\right). \tag{52}$$

It is straightforward to solve Equation 49 to obtain $\chi^1_{n,m,l,k}$. Substituting Equation 52 into Equation 46 gives:

$$\hat{\mathbf{q}}_{n,m,l,k}(r) = \chi^1_{n,m,l,k}(r) - \kappa_s / \left(2ma_{0,0} + 2kb_{0,0}\right) \hat{\mathbf{q}}_{n,0,l,0}(r). \tag{53}$$

In order to determine the Landau coefficients κ_s we use the normalizations in Equations 22 and 27. Together with the expansions in Equations 30 – 33 they require that:

$$|\tilde{u_r}^{1,0}(r_c, t)| = |\sum_{m=0}^{\infty}\sum_{k=0}^{\infty} A^{2m+1} B^{2k} \hat{u_r}^{1,m,0,k}(r_c)| = A(t) \tag{54}$$

and

$$|\tilde{u_r}^{0,1}(r_c, t)| = |\sum_{m=0}^{\infty}\sum_{k=0}^{\infty} A^{2m} B^{2k+1} \hat{u_r}^{0,m,1,k}(r_c)| = B(t). \tag{55}$$

We already used Equations 23 and 28 to set

$$\hat{u_r}^{1,0,0,0}(r_c) = 1$$

and

$$\hat{u_r}^{0,0,1,0}(r_c) = 1$$

hence for the normalization to be correct at all orders of approximation,

$$\hat{u_r}^{1,m,0,k}(r_c) = 0 \qquad \text{for all } m, k > 0 \tag{56}$$

and

$$\hat{u_r}^{0,m,1,k}(r_c) = 0 \qquad \text{for all } m, k > 0. \tag{57}$$

The conditions from Equations 56 and 57 can now be used to determine κ_s. Let the components of vector $\chi^1_{n,m,l,k}$ be written as:

$$\chi^1_{n,m,l,k} = \begin{pmatrix} \varpi_r \\ \varpi_\theta \\ \varpi_z \\ \varsigma \end{pmatrix}. \tag{58}$$

The conditions in Equations 56 and 57 are applied in Equation 53 to require:

$$\varpi_r(r_c) - \kappa_s / \left(2ma_{0,0} + 2kb_{0,0}\right) \hat{u_r}^{n,0,l,0}(r_c) = 0. \tag{59}$$

Since $\hat{u_r}^{n,0,l,0}(r_c) = 1$,

$$\kappa_s = \varpi_r(r_c)\left(2ma_{0,0} + 2kb_{0,0}\right). \tag{60}$$

Hence the Landau coefficients κ_s are determined. The correction to the fundamentals can be found by substitution back into Equation 46.

E. Numerical Considerations

All of the equation systems are solved using a Chebyshev collocation procedure [13]. The left-hand side operators for all of the systems (except the mean flow corrections) are similar and are generated with a single subroutine. The operators for the mean flow corrections need to ensure that only streamwise velocity perturbations are nonzero. This was most easily done using a separate subroutine. The right-hand side vectors were sufficiently different from each other that it was more convenient to use Macsyma to write individual subroutines for each of the equation systems. The two eigenproblems are solved first with a global solver to obtain the eigenvalue spectrum. The eigenvectors associated with the most unstable eigenvalue are obtained with a local iterative procedure. The mean flow needs to be computed using 128 bit accuracy for the very weak curvatures that we used. We found that 65 collocation points across the channel (including the endpoints) produced Landau coefficients which agreed to at least 3 digits with those obtained with 97 collocation points. All results presented here were obtained using 65 points.

F. Comparison of Approaches

Here we compare some aspects of the current approach with that of DHZ. Since they do not use the normalizations in Equations 22 and 27, they do not have the conditions of Equations 56 and 57 and hence need some alternative constraint to obtain Landau coefficients. They use orthogonality conditions to obtain the Landau coefficients when both Dean and TS disturbances are on their respective neutral stability curves. Near the neutral stability curves, the linear growth rates vary linearly with Reynolds number deviation off of the curves. Deviations from the critical curvature parameter, λ_c, are also assumed to affect the linear growth rates linearly. They find that the effect on the coefficients of the nonlinear terms in the Landau equations are independent of deviations away from the neutral Reynolds numbers and critical curvature to the order considered.

While the two approaches involve the same type of expansion, the different ways of solving for the Landau coefficients makes each appealing for obtaining certain types of information. Below we discuss some of the restrictions and advantages of each method.

Both theories assume that the fundamental disturbances are the major structures in the flow and that none of their harmonics or product wavevectors are linearly unstable. These secondary waves must be stable even in the presence of finite amplitude primary waves.

Both expansions are only valid for small amplitude disturbances. Exactly how small is not known *a priori*. In order for the expansions to be valid for large times, it is necessary for the linear growth rates to be "small". Small linear growth rates exist near the neutral stability curves. In this sense, the restriction of being near the neutral stability curves with the DHZ approach is similar to the requirement in the present approach that the amplitudes be small. The present approach might be somewhat more accurate if one were not interested

in long-time valid solutions; e.g. if one wanted only to know the first effect of nonlinearity on the strength of an instability. In such a case, the present amplitude expansion could be valid in cases with large linear growth rates as long as the amplitudes were still sufficiently small.

The theory developed by DHZ describes the weakly nonlinear behavior of the flow for a range of Reynolds number and curvature ratio perturbations away from the neutrally stable conditions. In particular, the perturbations could be taken into the linearly stable regime; there the Herbert approach may fail due to a resonance. The theory of DHZ does not have this problem since all of their constants are computed right on the neutral stability curves. On the other hand, the present theory may be applied to any combination of wavenumbers and Reynolds numbers, while the DHZ theory in its current form works only when the azimuthal and axial wavenumbers correspond to neutrally stable disturbances at the same Reynolds number.

The derivation and solution of the equations of the present theory are somewhat simpler than those of DHZ since the present theory does not require the use of adjoint eigenfunctions and the orthogonality condition. Additionally, because the amplitude function is uniquely defined in terms of the fundamental, the change in shape of the fundamental disturbance can be computed. This allows the present theory to be extended to higher orders unambiguously. Herbert [10] presents seven Landau constants for plane Poiseuille flow using this approach. With modified versions of the same procedure used here, Singer, Meyer, and Kleiser [14] and Ng, Singer, Henningson, and Alfredsson [15] compute multiple Landau coefficients for the development of vortices in a three-dimensional boundary layer and a rotating channel flow, respectively. Unfortunately, the derivation of the equations for the higher Landau coefficients for the present interacting wave case is too complicated to be handled within the framework of our current Macsyma program and is not done here.

III. Results

Most of our results are at the critical curvature parameter λ_c since this is where we expect the effects of the interaction to be greatest. Near the critical curvature parameter, $\lambda = \lambda_c = 2.179 \times 10^{-5}$, we found that small changes in the curvature parameter do not change the qualitative properties of the results. To orient the reader, Figures 2 and 3 are neutral stability curves for the TS and Dean waves respectively at the critical curvature. Regions where $a_{0,0}$ and $b_{0,0}$ are positive represent the linearly unstable areas. All of our results will be for points that are in the unstable regime of both the TS and Dean disturbances.

Figures 4 and 5 illustrate the zero contours of the Landau coefficients $a_{1,0}$ and $b_{0,1}$ in regions where the TS and Dean disturbances are linearly unstable, respectively. These coefficients represent the self-interaction effects of the TS and Dean disturbances. Positive values indicate that increased amplitude exasperates the instability. Negative values are necessary for an individual disturbance to reach a saturation state in the linearly unstable

region. The TS waves have negative self-interaction coefficients near the lower branch of the TS neutral stability curve, but positive values elsewhere. At low Reynolds numbers, the Dean disturbances have negative self-interaction coefficients for all wavenumbers β; at higher Reynolds numbers the self-interaction coefficient is positive in the middle of the unstable region.

Figures 6 and 7 indicate the effect that interaction has on the disturbances. In both of these figures, at a given Reynolds number, the right and left sides of the rectangle bound the streamwise wavenumber range in which individual 2D TS waves are linearly unstable. Similarly, for each Reynolds number, the top and bottom sides of the rectangle bound the spanwise wavenumber range in which Dean disturbances are linearly unstable . In Figure 6, positive values of $a_{0,1}$ indicate that the Dean disturbance has a destabilizing effect on the TS wave. This occurs primarily in the upper right hand corner of the unstable rectangle, though at high Reynolds numbers, there is also a small region of positive $a_{0,1}$ in the lower left corner. Where $a_{0,1}$ is positive in the upper right corner, the TS self-interaction coefficient $a_{1,0}$ is also positive, so the destabilizing effect of $a_{0,1}$ here exists when the TS wave by itself is already quite unstable. The Dean disturbance generally has a stabilizing effect on the TS waves at low Reynolds numbers, but as the Reynolds number increases, the Dean vortex has a destabilizing influence over a greater portion of the domain. The corresponding results for $b_{1,0}$, the effect of the TS wave on the Dean mode, are illustrated in Figure 7. Low wavenumber Dean disturbances tend to be destabilized by high wavenumber TS waves; however the fact that the harmonic of the Dean is also unstable in these cases invalidates the application of the theory here. In no case does the theory indicate that TS and Dean disturbances simultaneously destabilize each other. Since the coefficient, $b_{1,0}$ is positive over progressively smaller portions of the domain with increasing Reynolds number, it is unlikely that simultaneous destabilization occurs, even at very high Reynolds numbers. In most of the cases studied, the weakly nonlinear interaction tends to stabilize both modes. In a physical experiment, multiple three-dimensional modes can interact, perhaps forming a secondary instability which will eventually grow and lead to transition. A multi-wave interaction and subsequent instability is beyond the scope of the present theory.

For several representative sets of parameters, we examine our results in the context of nonlinear autonomous systems. Recall that A measures the amplitude of the TS wave and B corresponds to the Dean disturbance. Equations 35 and 36 admit four possible steady state solutions: the trivial solution, finite A with $B = 0$, finite B with $A = 0$, and a combined state with finite values of both A and B. Each of these states is a critical point and may be classified according to the local behavior of the solutions in the vicinity of the point. In the phase plane (A–B), stable nodes are identified as those for which solution trajectories near the point converge to the node, unstable nodes are critical points from which solution trajectories diverge, and saddle points are those points for which a finite number of trajectories converge to the point while all others diverge.

Several trajectories are illustrated in figure 8 for the case where Re $= 6291.67$, $\lambda = 2.189 \times 10^{-5}$, $\alpha = 74257$, and $\beta = 4.51$. These parameters were used extensively by Singer

and Zang [9] in their direct numerical simulations. In the figure, the small squares indicate the various initial conditions. An explicit fourth order Runge-Kutta differencing scheme was used to trace the subsequent trajectories. The filled circles show the two stable equilibrium points at $A = 3.8 \times 10^{-3}$, $B = 0$, and $A = 0$, $B = 7.0 \times 10^{-5}$ respectively. Trajectories initiated near either of these points tend to converge to the respective nodes. The open circles represent unstable nodes and saddle points. Two initial conditions started quite close to the saddle point at $A = 2.4 \times 10^{-4}$, $B = 3.5 \times 10^{-5}$ go to different stable equilibrium states. The flow is especially sensitive to small changes near the saddle point. The unstable node at the origin is the endpoint of a semi-infinite curve which goes through the saddle point and separates the region of attraction of the two stable nodes.

Figure 9 illustrates a typical trajectory for the case with Re = 4000, $\lambda = 2.179 \times 10^{-5}$, $\alpha = 96300$, and $\beta = 1.55$. In this case there are three critical points. The origin and $A = 0$, $B = 4.69 \times 10^{-5}$ are both unstable nodes. Trajectories that start in the vicinity of these points move away from them. The point $A = 3.8 \times 10^{-4}$, $B = 6.1 \times 10^{-5}$ is a stable spiral node. Trajectories slowly spiral towards this point. There is no conventional equilibrium point with $B = 0$ and $A \neq 0$. Trajectories initiated along this line will tend towards $A \rightarrow \infty$.

In the next case, the flow parameters are Re = 5000, $\lambda = 2.179 \times 10^{-5}$, $\alpha = 100000$, and $\beta = 2.0$. In Figure 10 pairs of trajectories with initial values of A differing by 0.001 are plotted for various initial values of B. In many ways, the qualitative behaviour seen here is quite similar to that illustrated in Figure 8. The origin is an unstable node, there is a saddle point with nonzero A and B, and there is a stable node with nonzero B but $A = 0$. A semi-infinite curve extends from the origin, through the saddle point and separates the domain into a region which is attracted to the stable node with $A = 0$, $B = 7.7 \times 10^{-4}$ and a region in which $A \rightarrow \infty$. This shows how strong the nonlinear interaction can be. Without a Dean disturbance, the TS wave has unbounded growth; however, the inclusion of an additional disturbance at sufficiently large amplitude can completely stabilize the otherwise growing TS wave.

We conclude this section by comparing our Landau coefficients with those of DHZ for two specific cases. Tables 2 and 3 show the Landau constants from the current theory and from the theory of DHZ after conversion to the current nondimensionalizations. The quantities $a_{0,0}$ and $b_{0,0}$ from DHZ were taken directly from their linear eigenvalue solver, rather than by perturbing away from the neutral stability curve. Except for the coefficient $b_{1,0}$, which represents the effect of the TS wave on the Dean disturbance, the coefficients show satisfactory agreement. Singer and Zang [9] suggested that a yet unknown numerical problem in DHZ led to erroneous values of $b_{1,0}$. The large discrepancy here with respect to $b_{1,0}$ adds support to that suggestion.

	$a_{0,0}$	$a_{1,0}$	$a_{0,1}$	$b_{0,0}$	$b_{1,0}$	$b_{0,1}$
Current	1.21×10^{-4}	-8.25	-95000	3.97×10^{-5}	-482	-7640
DHZ	1.20×10^{-4}	-8.85	-101000	3.97×10^{-5}	1.23×10^{5}	-8470

Table 2: Comparison of Landau Coefficients for Re = 6291.67, $\lambda = 2.189 \times 10^{-5}$, $\alpha = 74257$, and $\beta = 4.508$

	$a_{0,0}$	$a_{1,0}$	$a_{0,1}$	$b_{0,0}$	$b_{1,0}$	$b_{0,1}$
Current	1.18×10^{-5}	3.97	-46600	7.66×10^{-6}	-233	-3340
DHZ	1.33×10^{-5}	3.97	-46900	7.66×10^{-6}	1.44	-3390

Table 3: Comparison of Landau Coefficients for Re = 4175, $\lambda = 2.179 \times 10^{-5}$, $\alpha = 86800$, and $\beta = 2.76$

IV. Comparison with Direct Numerical Simulation

We use direct numerical simulations (DNS) of the full Navier-Stokes equations to determine the usefulness of the weakly nonlinear theory. The numerical simulation code [9] uses a curved channel variant of the method described by Zang and Hussaini [16] with the nonlinear terms in skew-symmetric form [17]. Table 4 reports the complex growth rates ($a_{0,0} - ig_{0,0}$) obtained with a spectral linear stability code, and the results of DNS with two different time steps. Table 5 provides details of the parameters for the different cases. All codes used 65 points across the channel. Data from the DNS were obtained after 100 time steps. Using a time step $\Delta t = 0.0001$, the complex growth rates differ from those predicted by linear theory by less than 1 part in 10^4. In the simulations reported below, we are primarily concerned with long-time trends and final steady-state solutions, hence, the additional time advancement errors associated with the larger time step, $\Delta t = 0.01$, are not expected to be important. The larger time step gave a maximum CFL number of 0.01, still well within the numerically stable regime. In one case described below, the time step was changed from $\Delta t = 0.01$ to $\Delta t = 0.0001$ after the steady state solution was reached. There was no evidence that the solution was changing, even after 20000 time steps. Additional details of code validation studies in both the linear and nonlinear regimes are given by Singer and Zang [9].

Case	Linear Stability	DNS $\Delta t = 0.01$	DNS $\Delta t = 0.0001$
1	(3.1189, −4236.9)	(3.0736, −4241.8)	(3.1185, −4236.9)
2	6.6331	6.6336	6.6335
3	(−138.2126, −16214.84)	(−138.2154, −16214.84)	(−138.2126, −16214.84)
4	(86.4287, −2709.11)	(86.4204, −2709.44)	(86.4291, −2709.14)
5	21.5591	21.5599	21.5599
6	(−90.61188, −12993.29)	(−90.61307, −12993.3)	(−90.61188, −12993.34)

Table 4: Comparison of Complex Growth Rates (all values multiplied by 10^4)

Case	Re	α	β
1	5000	100000	0
2	5000	0	2.0
3	5000	100000	2.0
4	10000	80000	0
5	10000	0	3.0
6	10000	80000	2.0

Table 5: Specification of parameters for cases in Table 4

Sufficient spatial resolution in the simulation can be ensured using the guideline suggested by Krist and Zang [18]. They suggest that "grid refinement is needed in any direction when the tail of the energy spectrum reaches 10^{-8} of the low-frequency value." This guarantees that truncation errors in the velocity will be less than 0.01%. Such detailed resolution is not necessary for the purposes of these simulations. We found that the tail of the energy spectrum could be as much as 10^{-4} of the low frequency value and still provide similar results to those obtained when the Krist and Zang guideline was strictly followed. Our relative insensitivity to resolution is attributed to the rather minor role that small scales play at this stage of transition. In what follows, using M Chebyshev modes implies that there are $M+1$ Chebyshev collocation points across the channel; using N Fourier modes implies that there are N collocation points in the given direction so that the Fourier wavenumbers, n, have a range of $-N/2+1 \leq nL/(2\pi) \leq N/2-1$, where L is the length of the domain. In most of the simulations with Re = 6291.67, 48 Chebyshev modes are used to resolve the flow in the wall-normal direction, though in the simulations with Re = 5000, 64 modes are used. In the streamwise and spanwise directions, 2–12 Fourier modes are used, depending on the purpose of the given simulation. The code is structured such that at least 2 modes must be used in each direction. In cases where no TS mode is included, 2 modes are used in the streamwise direction. Similarly, where no Dean mode is included, 2 modes are used in the spanwise direction.

The initial disturbances for the direct numerical simulations contain only contributions from the linear solutions. The distortion of the mean flow and higher harmonic contributions are not included initially; they develop as the simulation progresses.

Direct numerical simulation is used to study two of the three flows described in the previous section. The case in which there is a stable spiral mode is not simulated because the time required for a single orbit is so large that the computational cost would be prohibitive.

We first look at the case with Re = 6291.67, $\lambda = 2.189 \times 10^{-5}$, $\alpha = 74257$, and $\beta = 4.51$. Four simulations were performed with different initial conditions; the first contained only a Dean vortex, the second contained only a TS wave, the last two contained both types of disturbances.

When only a Dean disturbance is included in the initial conditions, the weakly nonlinear

theory suggests that an equilibrium state with $B = 7.0 \times 10^{-5}$ develops. This corresponds to a maximum streamwise velocity perturbation of 5.84% of $\overline{U^*}$. We initiated the simulation with the Dean eigenfunction obtained from linear stability theory with an initial strength, $B = 6.95 \times 10^{-5}$. Twelve Fourier modes were used in the spanwise direction, though half the modes had energies which were more than 8 orders of magnitude less than the primary mode. These higher order modes had a negligible effect on the simulation. At the start of the simulation, the instantaneous growth rate of the Dean disturbance was approximately equal to its linear value. At the time, $t = 34845$, the magnitude of the instantaneous growth rate had decreased by more than a factor of 100 and the simulation was stopped with $B = 6.7 \times 10^{-5}$. In this case, the difference between the equilibrium state predicted by the weakly nonlinear theory and that obtained from the DNS is less that 5% and is considered quite good.

With only a TS wave, we expect to obtain a TS equilibrium state with $A = 3.8 \times 10^{-3}$, resulting in a maximum streamwise disturbance of 1.94% of $\overline{U^*}$. The simulation was initiated with $A = 3.5 \times 10^{-3}$ and was stopped at a time $t = 11367$. At this time, $A = 4.0 \times 10^{-3}$. Figure 11 illustrates the time evolution of the amplitude of the wave. The dashed line shows the equilibrium amplitude predicted by our weakly nonlinear theory. Note that as the amplitude approaches its equilibrium value, the growth rate decreases. Over 480 periods of the TS wave were simulated for the data presented in Figure 11. The difference between the equilibrium amplitude predicted by the weakly nonlinear theory and that obtain by the DNS is about 10%, which we considered acceptable agreement. The 12 Fourier modes used in the streamwise direction were sufficient for an 8 order of magnitude drop in the energy.

We performed two simulations with both Dean and TS perturbations included in the initial conditions. In these, we used 6 modes in both the streamwise and spanwise directions and 48 Chebyshev modes in the wall-normal direction. In these simulations, the spanwise resolution was only sufficient to allow an energy drop of 10^5, while the streamwise resolution allowed as little as a 10^4 drop in the energy. This would lead us to suspect errors in the velocity on the order of 1%. To determine whether this could lead to erroneous physical results, we re-simulated our case which had the largest velocity perturbations using 12 modes in the streamwise and spanwise directions and 64 modes in the wall-normal direction. The energy spectrum in the highly resolved case exhibited an energy drop of 10^9 in the streamwise direction and 10^{14} in the spanwise direction. The evolution of the disturbance amplitudes was the same as that observed in the less resolved case. In both cases we initiated the Dean disturbances with $B = 6.95 \times 10^{-5}$. This value is slightly less than its equilibrium amplitude which we obtained above.

In the first case, the initial strength of the TS disturbance was $A = 2.94 \times 10^{-4}$, approximately 1/13 its predicted equilibrium value. The long time behavior of this case required 12 Fourier modes in the spanwise direction. The amplitude evolution of the disturbances is illustrated in Figure 12a. Here we plot the amplitude of both the Dean and TS disturbances, normalized by their respective amplitudes at time $t = 0$. The Dean disturbance develops towards its equilibrium state while the TS disturbance decays. In Figure 12b the predictions of

the weakly nonlinear theory are plotted. The agreement between the theoretical predictions and the DNS results is very good.

In the second case, the initial strength of the TS disturbance was $A = 2.94 \times 10^{-3}$, approximately 10/13 its predicted equilibrium value. Figure 13a shows the amplitude histories for this case. Unlike the previous situation, here it is the TS wave which grows towards its equilibrium value and the Dean disturbance which experiences rapid decay. The predictions of our weakly nonlinear theory are plotted in Figure 13b. Again the agreement between theory and simulation is quite good.

The next flow which we investigated with numerical simulations corresponds to the last case studied in the previous section. Here Re = 5000, $\lambda = \lambda_c = 2.179 \times 10^{-5}$, $\alpha = 100000$ and $\beta = 2.0$. Simulations were performed with a TS wave only, a Dean vortex only, and a combination of both disturbances.

The weakly nonlinear theory predicts that a TS wave alone in this flow becomes more unstable as its amplitude increases since both $a_{0,0}$ and $a_{1,0}$ are positive. A numerical simulation initiated with $A = 0.002$ and $B = 0$ confirmed that the amplitude A increased with increasing growth rate, at least until $A = 0.0048$ when the simulation was terminated. Six Fourier modes were used in the streamwise direction.

A Dean vortex alone in this flow is predicted to reach an equilibrium state with $B = 7.7 \times 10^{-4}$. This value of B corresponds to a maximum streamwise velocity perturbation which is 62.4% of the undisturbed laminar bulk velocity. An equilibrium state with $B = 4.3 \times 10^{-4}$ was obtained in the direct numerical simulations. Twelve Fourier modes were used in the spanwise direction. The difference between the DNS result and that of the weakly nonlinear theory is not unexpected since the disturbance amplitudes are so large.

One final simulation was performed with the initial values of A and B chosen as $A = 0.002$ and $B = 0.00065$. In this case, the weakly nonlinear theory predicts that the TS wave will decay, leaving only a Dean disturbance in the flow. The time evolutions of the TS and Dean disturbances are plotted in Figure 14a through $t = 500$. Six Fourier modes were used in the streamwise direction, twelve in the spanwise. At this time the spectral energy decay in the spanwise modes is 10^5. Though the simulation was terminated before a steady-state solution was reached, the prediction of the weakly nonlinear theory (plotted in Figure 14b is qualitatively supported. After the initial transient, the TS wave decays rapidly. Considering the large amplitude disturbances in the flow, the theory and the simulation agree well.

V. Conclusions

We have presented a weakly nonlinear theory to describe interactions between TS waves and Dean vortices in curved channel flow. The approach used to calculate the Landau coefficients is an extension of that developed by Herbert [10, 11]. This approach provides not only

the Landau coefficients, but also the shape change of the fundamental disturbances with amplitude. A standard Chebyshev collocation procedure is used to obtain numerical results. We have restricted our study to very weakly curved channels, where the critical Reynolds numbers for both TS and Dean disturbances are approximately equal. For low Reynolds numbers the interaction effects are generally stabilizing to both types of disturbances. In the case of high Reynolds numbers the theory predicts that the interaction can destabilize the TS wave. Destabilization of the Dean vortex due to the TS wave occurs only for very low wavenumber Dean disturbances.

Three different scenarios of TS-Dean interactions have been studied in detail. Phase plane trajectories indicate the existence of stable and unstable critical points. Two cases exhibit saddle point behaviour while the third has a stable spiral node.

Direct numerical simulations verify the predictions of the theory. When the amplitudes of the disturbances are not too large, the direct numerical simulations and the weakly nonlinear theory agree quite well. When the amplitudes of the disturbances are large (on the order of 60% of the centerline velocity), the simulations and the theory still qualitatively agree.

Comparison of our results with those of DHZ, who also developed a similar weakly nonlinear theory strongly suggest that DHZ have a numerical error in the computation of one of their Landau coefficients.

VI. Acknowledgements

The authors would like to thank Q. Isa Daudpota and Philip Hall for many useful discussions. NASA Langley Research Center supported B.A.S. under contract NAS1-18240.

I. The Left Hand Side Operator $\mathbf{L}_{n,l}$

$$\mathbf{L}_{n,l} = \begin{pmatrix} L^{1,1} & L^{1,2} & L^{1,3} & L^{1,4} \\ L^{2,1} & L^{2,2} & L^{2,3} & L^{2,4} \\ L^{3,1} & L^{3,2} & L^{3,3} & L^{3,4} \\ L^{4,1} & L^{4,2} & L^{4,3} & L^{4,4} \end{pmatrix}$$

$$\begin{aligned}
L^{1,1} &= i\alpha\frac{1}{r}U_\theta + \frac{1}{\mathrm{Re}}\left(l^2\beta^2 + (n^2\alpha^2+1)/r^2 - \frac{1}{r}\frac{d}{dr} - \frac{d^2}{dr^2}\right) \\
L^{1,2} &= -2\frac{U_\theta}{r} + \frac{2in\alpha}{r^2\mathrm{Re}} \\
L^{1,3} &= 0 \\
L^{1,4} &= \frac{d}{dr} \\
L^{2,1} &= \frac{dU_\theta}{dr} + \frac{U_\theta}{r} - \frac{2in\alpha}{r^2\mathrm{Re}} \\
L^{2,2} &= i\alpha\frac{1}{r}U_\theta + \frac{1}{\mathrm{Re}}\left(l^2\beta^2 + (n^2\alpha^2+1)/r^2 - \frac{1}{r}\frac{d}{dr} - \frac{d^2}{dr^2}\right) \\
L^{2,3} &= 0 \\
L^{2,4} &= i\frac{n\alpha}{r} \\
L^{3,1} &= 0 \\
L^{3,2} &= 0 \\
L^{3,3} &= i\alpha\frac{1}{r}U_\theta + \frac{1}{\mathrm{Re}}\left(l^2\beta^2 + n^2\alpha^2/r^2 - \frac{1}{r}\frac{d}{dr} - \frac{d^2}{dr^2}\right) \\
L^{3,4} &= il\beta \\
L^{4,1} &= \frac{1}{r} + \frac{d}{dr} \\
L^{4,2} &= i\frac{n\alpha}{r} \\
L^{4,3} &= il\beta \\
L^{4,4} &= 0
\end{aligned}$$

II. The Right Hand Side Vectors $\mathbf{R}_s$

$$\mathbf{R}_s = \begin{pmatrix} R_s^1 \\ R_s^2 \\ R_s^3 \\ R_s^4 \end{pmatrix}$$

Equation system 5 corresponds to the TS harmonic. Its right hand side vector is given by:

$$\begin{aligned}
R_5^1 &= -i\alpha \hat{u_\theta}^{1,0,0,0} \hat{u_r}^{1,0,0,0}/r \\
&\quad +(\hat{u_\theta}^{1,0,0,0})^2/r \\
&\quad -\frac{d}{dr}(\hat{u_r}^{1,0,0,0})\hat{u_r}^{1,0,0,0} \\
R_5^2 &= -i\alpha(\hat{u_\theta}^{1,0,0,0})^2/r \\
&\quad -\hat{u_\theta}^{1,0,0,0}\hat{u_r}^{1,0,0,0}/r \\
&\quad -\frac{d}{dr}(\hat{u_\theta}^{1,0,0,0})\hat{u_r}^{1,0,0,0} \\
R_5^3 &= -i\alpha \hat{u_\theta}^{1,0,0,0}\hat{u_z}^{1,0,0,0}/r \\
&\quad +\hat{u_r}^{1,0,0,0}\frac{d}{dr}(\hat{u_z}^{1,0,0,0}) \\
R_5^4 &= 0
\end{aligned}$$

Equation system 6 corresponds to the Dean harmonic. Its right hand side vector is given by:

$$\begin{aligned}
R_6^1 &= -i\beta \hat{u_z}^{0,0,1,0} \hat{u_r}^{0,0,1,0} \\
&\quad +(\hat{u_\theta}^{0,0,1,0})^2/r \\
&\quad -\frac{d}{dr}(\hat{u_r}^{0,0,1,0})\hat{u_r}^{0,0,1,0} \\
R_6^2 &= -i\beta \hat{u_\theta}^{0,0,1,0}\hat{u_z}^{0,0,1,0} \\
&\quad -\hat{u_\theta}^{0,0,1,0}\hat{u_r}^{0,0,1,0}/r \\
&\quad -\frac{d}{dr}(\hat{u_\theta}^{0,0,1,0})\hat{u_r}^{0,0,1,0} \\
R_6^3 &= -i\beta(\hat{u_z}^{0,0,1,0})^2 \\
&\quad +\hat{u_r}^{0,0,1,0}\frac{d}{dr}(\hat{u_z}^{0,0,1,0}) \\
R_6^4 &= 0
\end{aligned}$$

Equation system 7 corresponds to the product of the TS and Dean fundamentals. Its right hand side vector is given by:

$$R_7^1 = -i\alpha \hat{u_\theta}^{0,0,1,0}\hat{u_r}^{1,0,0,0}/r$$

$$
\begin{aligned}
& -i\beta \hat{u_r}^{0,0,1,0} \hat{u_z}^{1,0,0,0} \\
& +2\hat{u_\theta}^{0,0,1,0} \hat{u_\theta}^{1,0,0,0}/r \\
& -(\frac{d}{dr}(\hat{u_r}^{0,0,1,0})\hat{u_r}^{1,0,0,0} + \frac{d}{dr}(\hat{u_r}^{1,0,0,0})\hat{u_r}^{0,0,1,0}) \\
R_7^2 \;=\; & -i\alpha \hat{u_\theta}^{0,0,1,0} \hat{u_\theta}^{1,0,0,0}/r \\
& -i\beta \hat{u_\theta}^{0,0,1,0} \hat{u_z}^{1,0,0,0} \\
& -(\hat{u_\theta}^{0,0,1,0} \hat{u_r}^{1,0,0,0} + \hat{u_\theta}^{1,0,0,0} \hat{u_r}^{0,0,1,0})/r \\
& -(\frac{d}{dr}(\hat{u_\theta}^{0,0,1,0})\hat{u_r}^{1,0,0,0} + \frac{d}{dr}(\hat{u_\theta}^{1,0,0,0})\hat{u_r}^{0,0,1,0}) \\
R_7^3 \;=\; & -i\alpha \hat{u_\theta}^{0,0,1,0} \hat{u_z}^{1,0,0,0}/r \\
& -i\beta \hat{u_z}^{0,0,1,0} \hat{u_z}^{1,0,0,0} \\
& -(\frac{d}{dr}(\hat{u_z}^{0,0,1,0})\hat{u_r}^{1,0,0,0} + \frac{d}{dr}(\hat{u_z}^{1,0,0,0})\hat{u_r}^{0,0,1,0}) \\
R_7^4 \;=\; & 0
\end{aligned}
$$

Equation system 8 corresponds to the product of the TS fundamental and the complex conjugate of the Dean fundamental. Its right hand side vector is given by:

$$
\begin{aligned}
R_8^1 \;=\; & -i\alpha \hat{u_\theta}^{0,0,-1,0} \hat{u_r}^{1,0,0,0}/r \\
& +i\beta \hat{u_r}^{0,0,-1,0} \hat{u_z}^{1,0,0,0} \\
& +2\hat{u_\theta}^{0,0,-1,0} \hat{u_\theta}^{1,0,0,0}/r \\
& -(\frac{d}{dr}(\hat{u_r}^{0,0,-1,0})\hat{u_r}^{1,0,0,0} + \frac{d}{dr}(\hat{u_r}^{1,0,0,0})\hat{u_r}^{0,0,-1,0}) \\
R_8^2 \;=\; & -i\alpha \hat{u_\theta}^{0,0,-1,0} \hat{u_\theta}^{1,0,0,0}/r \\
& +i\beta \hat{u_\theta}^{0,0,-1,0} \hat{u_z}^{1,0,0,0} \\
& -(\hat{u_\theta}^{0,0,-1,0} \hat{u_r}^{1,0,0,0} + \hat{u_\theta}^{1,0,0,0} \hat{u_r}^{0,0,-1,0})/r \\
& -(\frac{d}{dr}(\hat{u_\theta}^{0,0,-1,0})\hat{u_r}^{1,0,0,0} + \frac{d}{dr}(\hat{u_\theta}^{1,0,0,0})\hat{u_r}^{0,0,-1,0}) \\
R_8^3 \;=\; & -i\alpha \hat{u_\theta}^{0,0,-1,0} \hat{u_z}^{1,0,0,0}/r \\
& +i\beta \hat{u_z}^{0,0,-1,0} \hat{u_z}^{1,0,0,0} \\
& -(\frac{d}{dr}(\hat{u_z}^{0,0,-1,0})\hat{u_r}^{1,0,0,0} + \frac{d}{dr}(\hat{u_z}^{1,0,0,0})\hat{u_r}^{0,0,-1,0}) \\
R_8^4 \;=\; & 0
\end{aligned}
$$

Equation system 9 corresponds to the self correction of the TS fundamental. Its right hand side vector is given by:

$$
\begin{aligned}
R_9^1 \;=\; & -i\alpha(2\hat{u_\theta}^{-1,0,0,0} \hat{u_r}^{2,0,0,0} + \hat{u_\theta}^{0,1,0,0} \hat{u_r}^{1,0,0,0} - \hat{u_\theta}^{2,0,0,0} \hat{u_r}^{-1,0,0,0})/r \\
& +(2\hat{u_\theta}^{-1,0,0,0} \hat{u_\theta}^{2,0,0,0} + 2\hat{u_\theta}^{0,1,0,0} \hat{u_\theta}^{1,0,0,0})/r \\
& -(\frac{d}{dr}(\hat{u_r}^{2,0,0,0})\hat{u_r}^{-1,0,0,0} + \frac{d}{dr}(\hat{u_r}^{-1,0,0,0})\hat{u_r}^{2,0,0,0}
\end{aligned}
$$

$$
\begin{aligned}
& +\frac{d}{dr}(\hat{u_r}^{0,1,0,0})\hat{u_r}^{1,0,0,0} + \frac{d}{dr}(\hat{u_r}^{1,0,0,0})\hat{u_r}^{0,1,0,0}) \\
& -(a_{1,0} - ig_{1,0})\hat{u_r}^{1,0,0,0} \\
R_9^2 \;=\; & -i\alpha(\hat{u_\theta}^{-1,0,0,0}\hat{u_\theta}^{2,0,0,0} + \hat{u_\theta}^{0,1,0,0}\hat{u_\theta}^{1,0,0,0})/r \\
& -(\hat{u_\theta}^{-1,0,0,0}\hat{u_r}^{2,0,0,0} + \hat{u_\theta}^{2,0,0,0}\hat{u_r}^{-1,0,0,0} + \hat{u_\theta}^{0,1,0,0}\hat{u_r}^{1,0,0,0} + \hat{u_\theta}^{1,0,0,0}\hat{u_r}^{0,1,0,0})/r \\
& -(\frac{d}{dr}(\hat{u_\theta}^{-1,0,0,0})\hat{u_r}^{2,0,0,0} + \frac{d}{dr}(\hat{u_\theta}^{2,0,0,0})\hat{u_r}^{-1,0,0,0} \\
& +\frac{d}{dr}(\hat{u_\theta}^{0,1,0,0})\hat{u_r}^{1,0,0,0} + \frac{d}{dr}(\hat{u_\theta}^{1,0,0,0})\hat{u_r}^{0,1,0,0}) \\
& -(a_{1,0} - ig_{1,0})\hat{u_\theta}^{1,0,0,0} \\
R_9^3 \;=\; & -i\alpha(2\hat{u_\theta}^{-1,0,0,0}\hat{u_z}^{2,0,0,0} + \hat{u_\theta}^{0,1,0,0}\hat{u_z}^{1,0,0,0} - \hat{u_\theta}^{2,0,0,0}\hat{u_z}^{-1,0,0,0})/r \\
& -(\frac{d}{dr}(\hat{u_z}^{-1,0,0,0})\hat{u_r}^{2,0,0,0} + \frac{d}{dr}(\hat{u_z}^{2,0,0,0})\hat{u_r}^{-1,0,0,0} \\
& +\frac{d}{dr}(\hat{u_z}^{0,1,0,0})\hat{u_r}^{1,0,0,0} + \frac{d}{dr}(\hat{u_z}^{1,0,0,0})\hat{u_r}^{0,1,0,0}) \\
& -(a_{1,0} - ig_{1,0})\hat{u_z}^{1,0,0,0} \\
R_9^4 \;=\; & 0
\end{aligned}
$$

Equation system 10 corresponds to the self correction of the Dean fundamental. Its right hand side vector is given by:

$$
\begin{aligned}
R_{10}^1 \;=\; & -i\beta(2\hat{u_z}^{0,0,-1,0}\hat{u_r}^{0,0,2,0} + \hat{u_z}^{0,0,0,1}\hat{u_r}^{0,0,1,0} - \hat{u_z}^{0,0,2,0}\hat{u_r}^{0,0,-1,0}) \\
& +(2\hat{u_\theta}^{0,0,-1,0}\hat{u_\theta}^{0,0,2,0} + 2\hat{u_\theta}^{0,0,0,1}\hat{u_\theta}^{0,0,1,0})/r \\
& -(\frac{d}{dr}(\hat{u_r}^{0,0,2,0})\hat{u_r}^{0,0,-1,0} + \frac{d}{dr}(\hat{u_r}^{0,0,-1,0})\hat{u_r}^{0,0,2,0} \\
& +\frac{d}{dr}(\hat{u_r}^{0,0,0,1})\hat{u_r}^{0,0,1,0} + \frac{d}{dr}(\hat{u_r}^{0,0,1,0})\hat{u_r}^{0,0,0,1}) \\
& -(b_{0,1} - ih_{0,1})\hat{u_r}^{0,0,1,0} \\
R_{10}^2 \;=\; & -i\beta(2\hat{u_\theta}^{0,0,2,0}\hat{u_z}^{0,0,-1,0} + \hat{u_\theta}^{0,0,1,0}\hat{u_z}^{0,0,0,1} - \hat{u_\theta}^{0,0,-1,0}\hat{u_z}^{0,0,2,0}) \\
& -(\hat{u_\theta}^{0,0,-1,0}\hat{u_r}^{0,0,2,0} + \hat{u_\theta}^{0,0,2,0}\hat{u_r}^{0,0,-1,0} \\
& +\hat{u_\theta}^{0,0,0,1}\hat{u_r}^{0,0,1,0} + \hat{u_\theta}^{0,0,1,0}\hat{u_r}^{0,0,0,1})/r \\
& -(\frac{d}{dr}(\hat{u_\theta}^{0,0,-1,0})\hat{u_r}^{0,0,2,0} + \frac{d}{dr}(\hat{u_\theta}^{0,0,2,0})\hat{u_r}^{0,0,-1,0} \\
& +\frac{d}{dr}(\hat{u_\theta}^{0,0,0,1})\hat{u_r}^{0,0,1,0} + \frac{d}{dr}(\hat{u_\theta}^{0,0,1,0})\hat{u_r}^{0,0,0,1}) \\
& -(b_{0,1} - ih_{0,1})\hat{u_\theta}^{0,0,1,0} \\
R_{10}^3 \;=\; & -i\beta(\hat{u_z}^{0,0,-1,0}\hat{u_z}^{0,0,2,0} + \hat{u_z}^{0,0,0,1}\hat{u_z}^{0,0,1,0}) \\
& -(\frac{d}{dr}(\hat{u_z}^{0,0,-1,0})\hat{u_r}^{0,0,2,0} + \frac{d}{dr}(\hat{u_z}^{0,0,2,0})\hat{u_r}^{0,0,-1,0} \\
& +\frac{d}{dr}(\hat{u_z}^{0,0,0,1})\hat{u_r}^{0,0,1,0} + \frac{d}{dr}(\hat{u_z}^{0,0,1,0})\hat{u_r}^{0,0,0,1}) \\
& -(b_{0,1} - ih_{0,1})\hat{u_z}^{0,0,1,0}
\end{aligned}
$$

$$R_{10}^4 = 0$$

Equation system 11 corresponds to the correction of the TS fundamental by the Dean. Its right hand side vector is given by:

$$\begin{aligned}
R_{11}^1 = & -i\alpha(\hat{u_\theta}^{0,0,-1,0}\hat{u_r}^{1,0,1,0} + \hat{u_\theta}^{0,0,0,1}\hat{u_r}^{1,0,0,0} + \hat{u_\theta}^{0,0,1,0}\hat{u_r}^{1,0,-1,0})/r \\
& +i\beta(\hat{u_r}^{0,0,-1,0}\hat{u_z}^{1,0,1,0} - \hat{u_r}^{0,0,1,0}\hat{u_z}^{1,0,-1,0} \\
& +\hat{u_r}^{1,0,-1,0}\hat{u_z}^{0,0,1,0} - \hat{u_r}^{1,0,1,0}\hat{u_z}^{0,0,-1,0}) \\
& +2(\hat{u_\theta}^{0,0,-1,0}\hat{u_\theta}^{1,0,1,0} + \hat{u_\theta}^{0,0,0,1}\hat{u_\theta}^{1,0,0,0} + \hat{u_\theta}^{0,0,1,0}\hat{u_\theta}^{1,0,-1,0})/r \\
& -(\frac{d}{dr}(\hat{u_r}^{0,0,-1,0})\hat{u_r}^{1,0,1,0} + \frac{d}{dr}(\hat{u_r}^{0,0,0,1})\hat{u_r}^{1,0,0,0} \\
& +\frac{d}{dr}(\hat{u_r}^{0,0,1,0})\hat{u_r}^{1,0,-1,0} + \frac{d}{dr}(\hat{u_r}^{1,0,-1,0})\hat{u_r}^{0,0,1,0} \\
& +\frac{d}{dr}(\hat{u_r}^{1,0,0,0})\hat{u_r}^{0,0,0,1} + \frac{d}{dr}(\hat{u_r}^{1,0,1,0})\hat{u_r}^{0,0,-1,0}) \\
& -(a_{0,1} - ig_{0,1})\hat{u_r}^{1,0,0,0} \\
R_{11}^2 = & -i\alpha(\hat{u_\theta}^{0,0,-1,0}\hat{u_\theta}^{1,0,1,0} + \hat{u_\theta}^{0,0,0,1}\hat{u_\theta}^{1,0,0,0} + \hat{u_\theta}^{0,0,1,0}\hat{u_\theta}^{1,0,-1,0})/r \\
& +i\beta(\hat{u_\theta}^{0,0,-1,0}\hat{u_z}^{1,0,1,0} - \hat{u_\theta}^{0,0,1,0}\hat{u_z}^{1,0,-1,0} \\
& +\hat{u_\theta}^{1,0,-1,0}\hat{u_z}^{0,0,1,0} - \hat{u_\theta}^{1,0,1,0}\hat{u_z}^{0,0,-1,0}) \\
& -(\hat{u_\theta}^{0,0,-1,0}\hat{u_r}^{1,0,1,0} + \hat{u_\theta}^{0,0,0,1}\hat{u_r}^{1,0,0,0} \\
& +\hat{u_\theta}^{0,0,1,0}\hat{u_r}^{1,0,-1,0} + \hat{u_\theta}^{1,0,-1,0}\hat{u_r}^{0,0,1,0} \\
& +\hat{u_\theta}^{1,0,0,0}\hat{u_r}^{0,0,0,1} + \hat{u_\theta}^{1,0,1,0}\hat{u_r}^{0,0,-1,0})/r \\
& -(\frac{d}{dr}(\hat{u_\theta}^{0,0,-1,0})\hat{u_r}^{1,0,1,0} + \frac{d}{dr}(\hat{u_\theta}^{0,0,0,1})\hat{u_r}^{1,0,0,0} \\
& +\frac{d}{dr}(\hat{u_\theta}^{0,0,1,0})\hat{u_r}^{1,0,-1,0} + \frac{d}{dr}(\hat{u_\theta}^{1,0,-1,0})\hat{u_r}^{0,0,1,0} \\
& +\frac{d}{dr}(\hat{u_\theta}^{1,0,0,0})\hat{u_r}^{0,0,0,1} + \frac{d}{dr}(\hat{u_\theta}^{1,0,1,0})\hat{u_r}^{0,0,-1,0}) \\
& -(a_{0,1} - ig_{0,1})\hat{u_\theta}^{1,0,0,0} \\
R_{11}^3 = & -i\alpha(\hat{u_\theta}^{0,0,-1,0}\hat{u_z}^{1,0,1,0} + \hat{u_\theta}^{0,0,0,1}\hat{u_z}^{1,0,0,0} + \hat{u_\theta}^{0,0,1,0}\hat{u_z}^{1,0,-1,0})/r \\
& -(\frac{d}{dr}(\hat{u_z}^{0,0,-1,0})\hat{u_r}^{1,0,1,0} + \frac{d}{dr}(\hat{u_z}^{0,0,0,1})\hat{u_r}^{1,0,0,0} \\
& +\frac{d}{dr}(\hat{u_z}^{0,0,1,0})\hat{u_r}^{1,0,-1,0} + \frac{d}{dr}(\hat{u_z}^{1,0,-1,0})\hat{u_r}^{0,0,1,0} \\
& +\frac{d}{dr}(\hat{u_z}^{1,0,0,0})\hat{u_r}^{0,0,0,1} + \frac{d}{dr}(\hat{u_z}^{1,0,1,0})\hat{u_r}^{0,0,-1,0}) \\
& -(a_{0,1} - ig_{0,1})\hat{u_z}^{1,0,0,0} \\
R_{11}^4 = & \ 0
\end{aligned}$$

Equation system 12 corresponds to the correction of the Dean fundamental by the TS. Its right hand side vector is given by:

$$R_{12}^1 = -i\alpha(\hat{u_\theta}^{-1,0,0,0}\hat{u_r}^{1,0,1,0} + \hat{u_\theta}^{-1,0,1,0}\hat{u_r}^{1,0,0,0} - \hat{u_\theta}^{1,0,0,0}\hat{u_r}^{-1,0,1,0} + \hat{u_\theta}^{1,0,1,0}\hat{u_r}^{-1,0,0,0})/r$$

$$
\begin{aligned}
& -i\beta(\hat{u_r}^{-1,0,1,0}\hat{u_z}^{1,0,0,0} + \hat{u_r}^{0,0,1,0}\hat{u_z}^{0,1,0,0} + \hat{u_r}^{1,0,1,0}\hat{u_z}^{-1,0,0,0}) \\
& +2(\hat{u_\theta}^{-1,0,0,0}\hat{u_\theta}^{1,0,1,0} + \hat{u_\theta}^{-1,0,1,0}\hat{u_\theta}^{1,0,0,0} + \hat{u_\theta}^{0,0,1,0}\hat{u_\theta}^{0,1,0,0})/r \\
& -(\frac{d}{dr}(\hat{u_r}^{-1,0,0,0})\hat{u_r}^{1,0,1,0} + \frac{d}{dr}(\hat{u_r}^{-1,0,1,0})\hat{u_r}^{1,0,0,0} \\
& +\frac{d}{dr}(\hat{u_r}^{0,0,1,0})\hat{u_r}^{0,1,0,0} + \frac{d}{dr}(\hat{u_r}^{0,1,0,0})\hat{u_r}^{0,0,1,0} \\
& +\frac{d}{dr}(\hat{u_r}^{1,0,0,0})\hat{u_r}^{-1,0,1,0} + \frac{d}{dr}(\hat{u_r}^{1,0,1,0})\hat{u_r}^{-1,0,0,0}) \\
& -(b_{1,0} - ih_{1,0})\hat{u_r}^{0,0,1,0}
\end{aligned}
$$

$$
\begin{aligned}
R_{12}^2 = & -i\beta(\hat{u_\theta}^{-1,0,1,0}\hat{u_z}^{1,0,0,0} + \hat{u_\theta}^{0,0,1,0}\hat{u_z}^{0,1,0,0} + \hat{u_\theta}^{1,0,1,0}\hat{u_z}^{-1,0,0,0}) \\
& -(\hat{u_\theta}^{-1,0,0,0}\hat{u_r}^{1,0,1,0} + \hat{u_\theta}^{-1,0,1,0}\hat{u_r}^{1,0,0,0} \\
& +\hat{u_\theta}^{0,0,1,0}\hat{u_r}^{0,1,0,0} + \hat{u_\theta}^{0,1,0,0}\hat{u_r}^{0,0,1,0} \\
& +\hat{u_\theta}^{1,0,0,0}\hat{u_r}^{-1,0,1,0} + \hat{u_\theta}^{1,0,1,0}\hat{u_r}^{-1,0,0,0})/r \\
& -(\frac{d}{dr}(\hat{u_\theta}^{-1,0,0,0})\hat{u_r}^{1,0,1,0} + \frac{d}{dr}(\hat{u_\theta}^{-1,0,1,0})\hat{u_r}^{1,0,0,0} \\
& +\frac{d}{dr}(\hat{u_\theta}^{0,0,1,0})\hat{u_r}^{0,1,0,0} + \frac{d}{dr}(\hat{u_\theta}^{0,1,0,0})\hat{u_r}^{0,0,1,0} \\
& +\frac{d}{dr}(\hat{u_\theta}^{1,0,0,0})\hat{u_r}^{-1,0,1,0} + \frac{d}{dr}(\hat{u_\theta}^{1,0,1,0})\hat{u_r}^{-1,0,0,0}) \\
& -(b_{1,0} - ih_{1,0})\hat{u_\theta}^{0,0,1,0}
\end{aligned}
$$

$$
\begin{aligned}
R_{12}^3 = & -i\alpha(\hat{u_\theta}^{-1,0,0,0}\hat{u_z}^{1,0,1,0} + \hat{u_\theta}^{-1,0,1,0}\hat{u_z}^{1,0,0,0} - \hat{u_\theta}^{1,0,0,0}\hat{u_z}^{-1,0,1,0} - \hat{u_\theta}^{1,0,1,0}\hat{u_z}^{-1,0,0,0})/r \\
& -i\beta(\hat{u_z}^{-1,0,1,0}\hat{u_z}^{1,0,0,0} + \hat{u_z}^{0,0,1,0}\hat{u_z}^{0,1,0,0} + \hat{u_z}^{1,0,1,0}\hat{u_z}^{-1,0,0,0}) \\
& -(\frac{d}{dr}(\hat{u_z}^{-1,0,0,0})\hat{u_r}^{1,0,1,0} + \frac{d}{dr}(\hat{u_z}^{-1,0,1,0})\hat{u_r}^{1,0,0,0} \\
& +\frac{d}{dr}(\hat{u_z}^{0,0,1,0})\hat{u_r}^{0,1,0,0} + \frac{d}{dr}(\hat{u_z}^{0,1,0,0})\hat{u_r}^{0,0,1,0} \\
& +\frac{d}{dr}(\hat{u_z}^{1,0,0,0}\hat{u_r}^{-1,0,1,0} + \frac{d}{dr}(\hat{u_z}^{1,0,1,0})\hat{u_r}^{-1,0,0,0}) \\
& -(b_{1,0} - ih_{1,0})\hat{u_z}^{0,0,1,0}
\end{aligned}
$$

$$
R_{12}^4 = 0
$$

References

[1] Dean, W.R. 1928: Fluid Motion in a Curved Channel, *Proc. Roy. Soc. London A* **121:** pp. 402–420.

[2] Reid, W.H. 1954: On the Stability of Viscous Flow in a Curved Channel, *Proc. Roy. Soc. London A* **244:** p 186.

[3] Ligrani, P. M.; Niver, R. D. 1988: Flow Visualization of Dean Vortices in a Curved Channel with 40 to 1 Aspect Ratio, *Phy. Fl.* **31:** pp. 3605 - 3617.

[4] Finlay, Warren H.; Keller, Joseph B.; and Ferziger, Joel H. 1988: Instability and Transition in Curved Channel Flow, *J. Fluid Mech.* **194:** pp. 417–456.

[5] Gibson, R.D.; and Cook, A.E. 1974: The Stability of Curved Channel Flow, *Quarterly J. of Mech. and Applied Math.* **27:** pp. 149–160.

[6] Daudpota, Q. Isa; Hall, Philip; and Zang, Thomas A. 1988: On the Nonlinear Interaction of Gortler Vortices and Tollmien-Schlichting Waves in Curved Channel Flows at Finite Reynolds Numbers, *J. Fluid Mech.* **193:** pp. 569–595.

[7] Stuart, J.T. 1960: On the Nonlinear Mechanics of Wave Disturbances in Stable and Unstable Parallel Flows. Part 1. The Basic Behaviour in Plane Poiseuille Flow, *J. Fluid Mech.* **9:** pp 353–370.

[8] Watson, J. 1960: On the Nonlinear Mechanics of Wave Disturbances in Stable and Unstable Parallel Flows. Part 2. The Development of a Solution for Plane Poiseuille Flow and for Plane Couette Flow, *J. Fluid Mech.* **9:** pp 371–389.

[9] Singer, B.A.; and Zang, T.A. 1989: Direct Numerical Simulations of Tollmien-Schlichting/Dean Interactions. NASA *Technical Paper 2919.*

[10] Herbert, Thorwald 1980: Nonlinear Stability of Parallel Flows by High-Order Amplitude Expansions, *AIAA J.* **18:** pp 243–248.

[11] Herbert, Thorwald 1983: On Perturbation Methods in Nonlinear Stability Theory, *J. Fluid Mech.* **126:** pp 167–186.

[12] Drazin, P.G. and Reid, W.H. 1982: *Hydrodynamic Stability.* p. 384.

[13] Gottlieb, D. and Orszag, S.A. 1981: *Numerical Analysis of Spectral Methods: Theory and Applications*, Publ. Siam.

[14] Singer, B.A.; Meyer, F.; and Kleiser, L. 1989: Nonlinear Development of Crossflow Vortices, *Instability and Transition (ICASE/NASA)*, eds. Hussaini, M. and Voigt, R., Springer, New York.

[15] Ng, L., Singer, B.A., Henningson, D.S., and Alfredsson, P.H.; 1989: Instabilities in Rotating Channel Flow, *Instability and Transition (ICASE/NASA)*, eds. Hussaini, M. and Voigt, R., Springer, New York.

[16] Zang, Thomas A.; and Hussaini, M. Yousuff 1986: On Spectral Multigrid Methods for the Time-Dependent Navier Stokes Equations, *Applied Math. and Comp.* **19:** pp. 359–372.

[17] Zang, Thomas A. 1990: On the Rotation and Skew-Symmetric Forms for Incompressible Flow Simulations, *Appl. Numer. Math.*, **6.**

[18] Krist, Steven E.; and Zang, Thomas A. 1987: Numerical Simulation of Channel Flow Transition: Resolution Requirements and Structure of the Hairpin Vortex, NASA *Technical Paper 2667,* Apr.

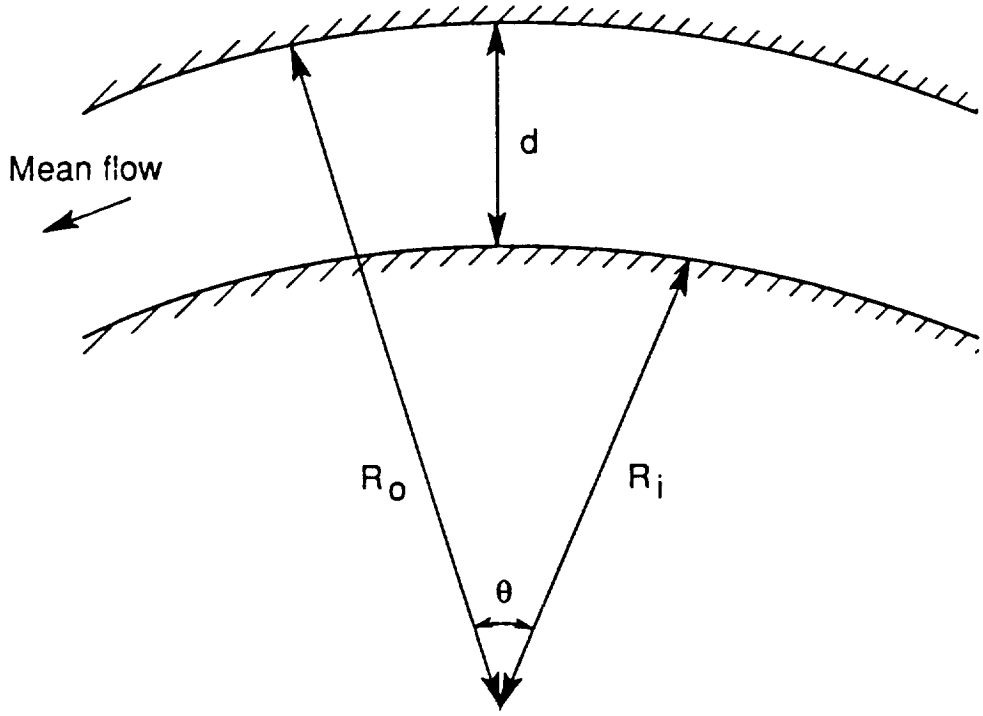

Figure 1: Curved channel flow geometry.

Figure 2

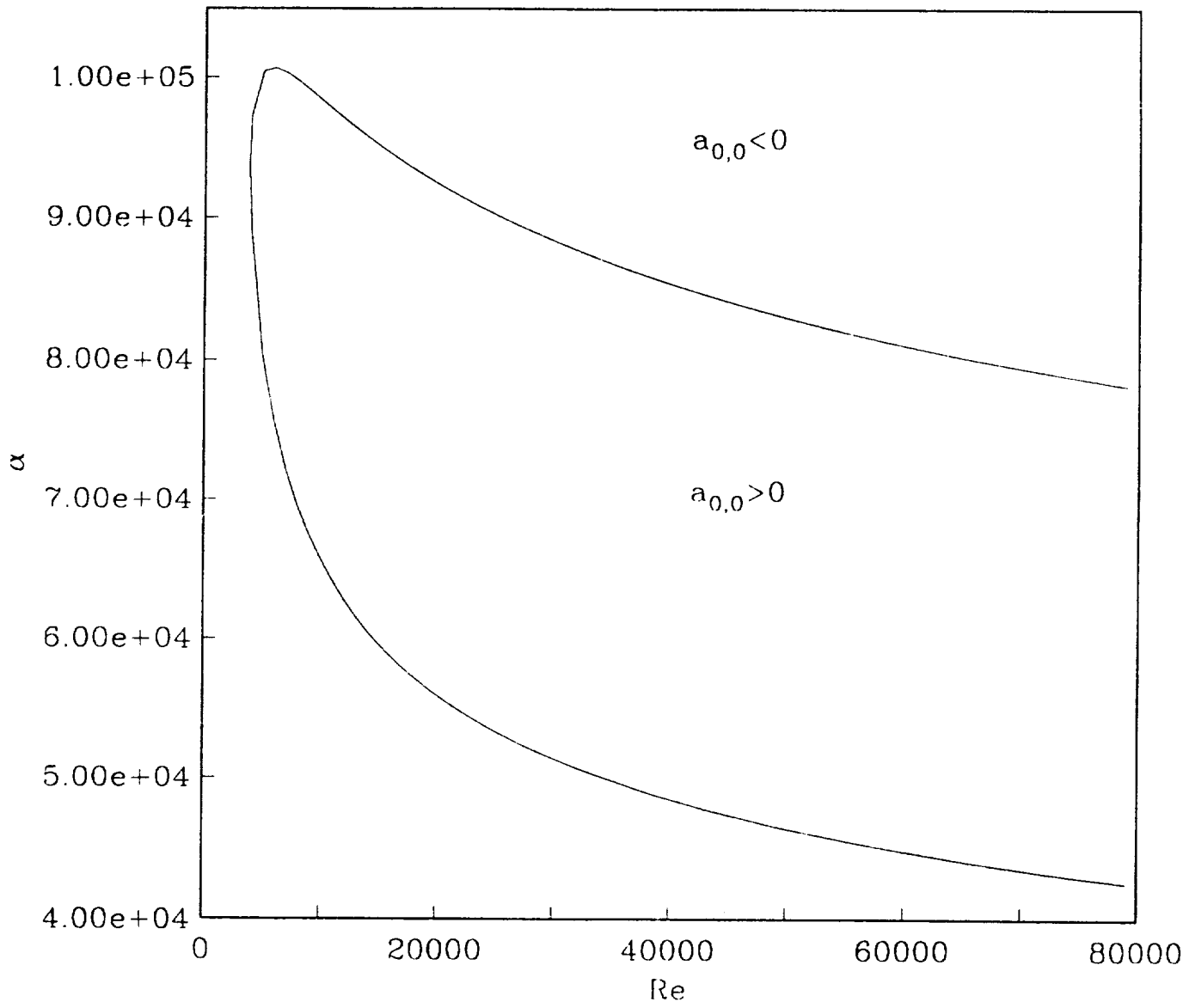

Figure 2: TS neutral stability curve with $\lambda = \lambda_c = 2.179 \times 10^{-5}$.

Figure 3

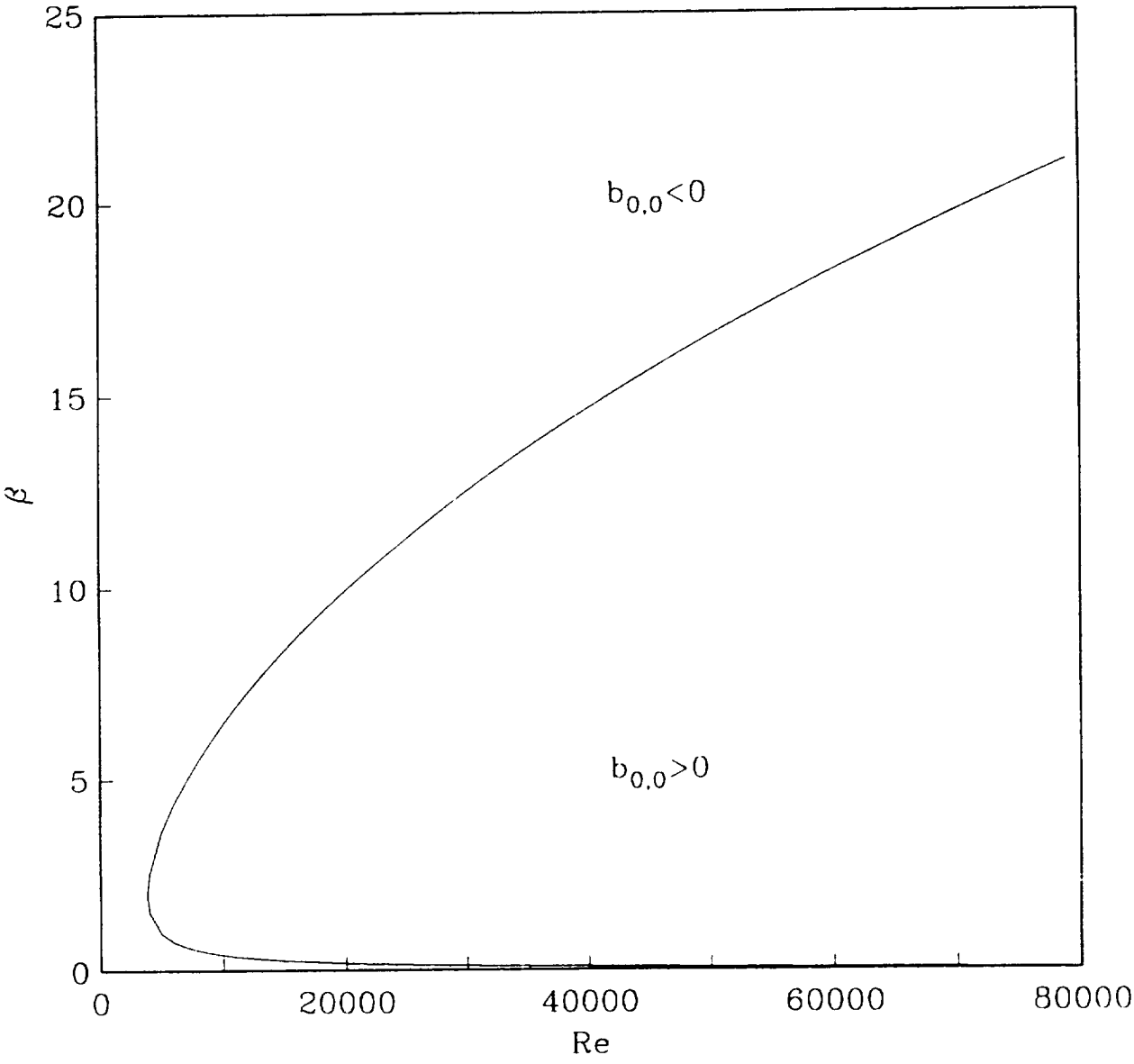

Figure 3: Dean neutral stability curve with $\lambda = \lambda_c = 2.179 \times 10^{-5}$.

Figure 4

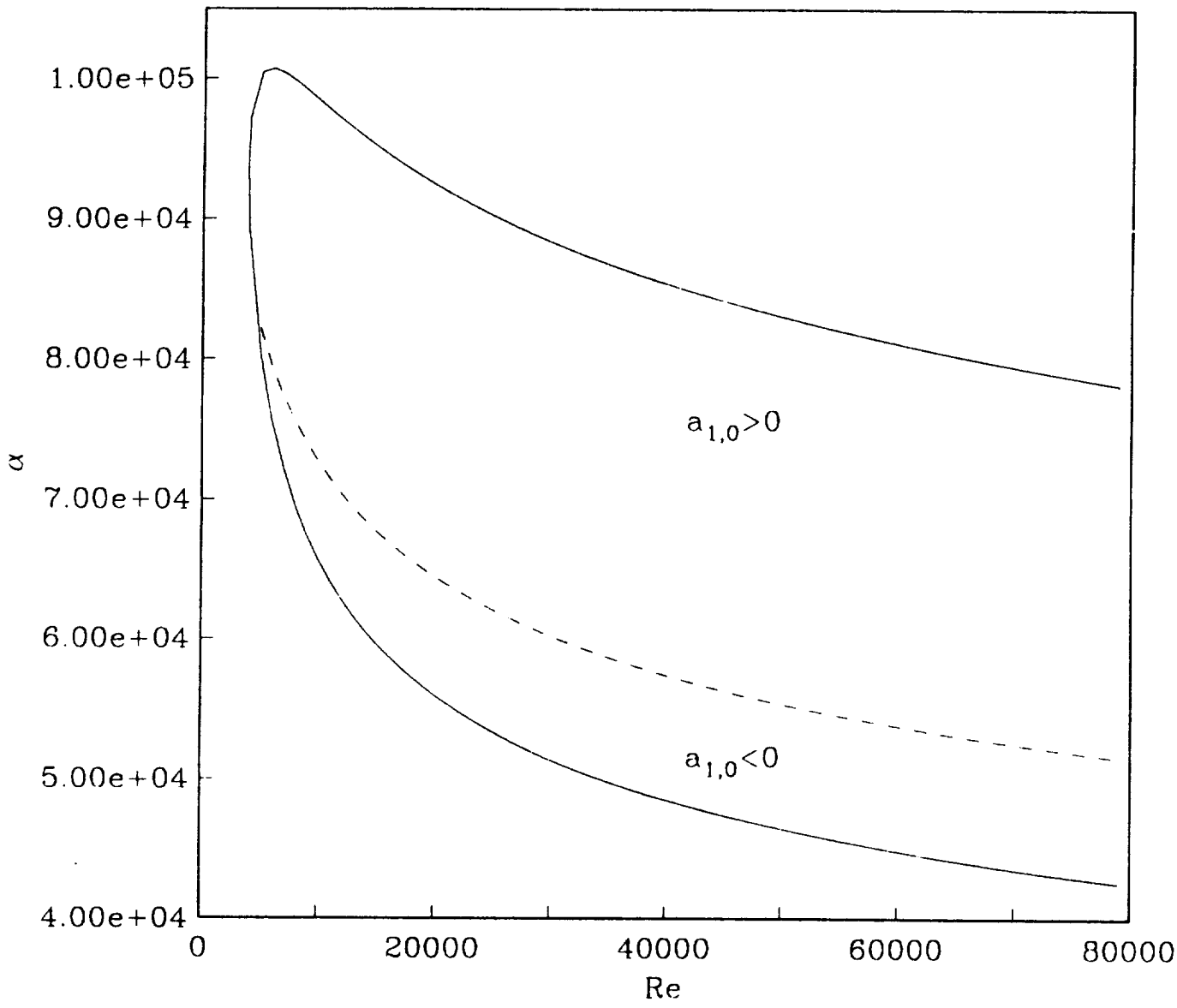

Figure 4: Zero contour of $a_{1,0}$, the TS self-interaction coefficient.

Figure 5

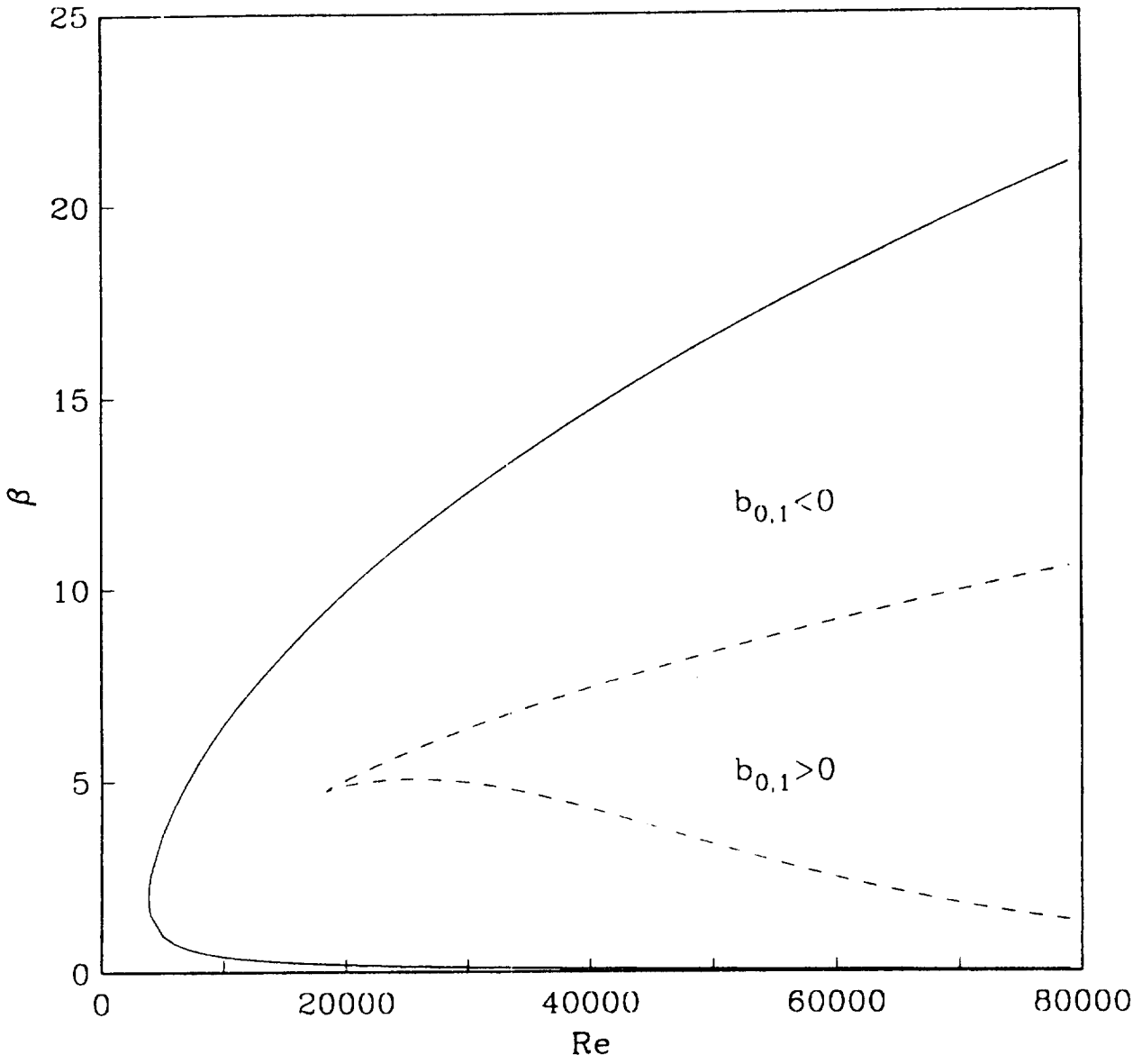

Figure 5: Zero contour of $b_{0,1}$, the Dean self-interaction coefficient.

Figure 6

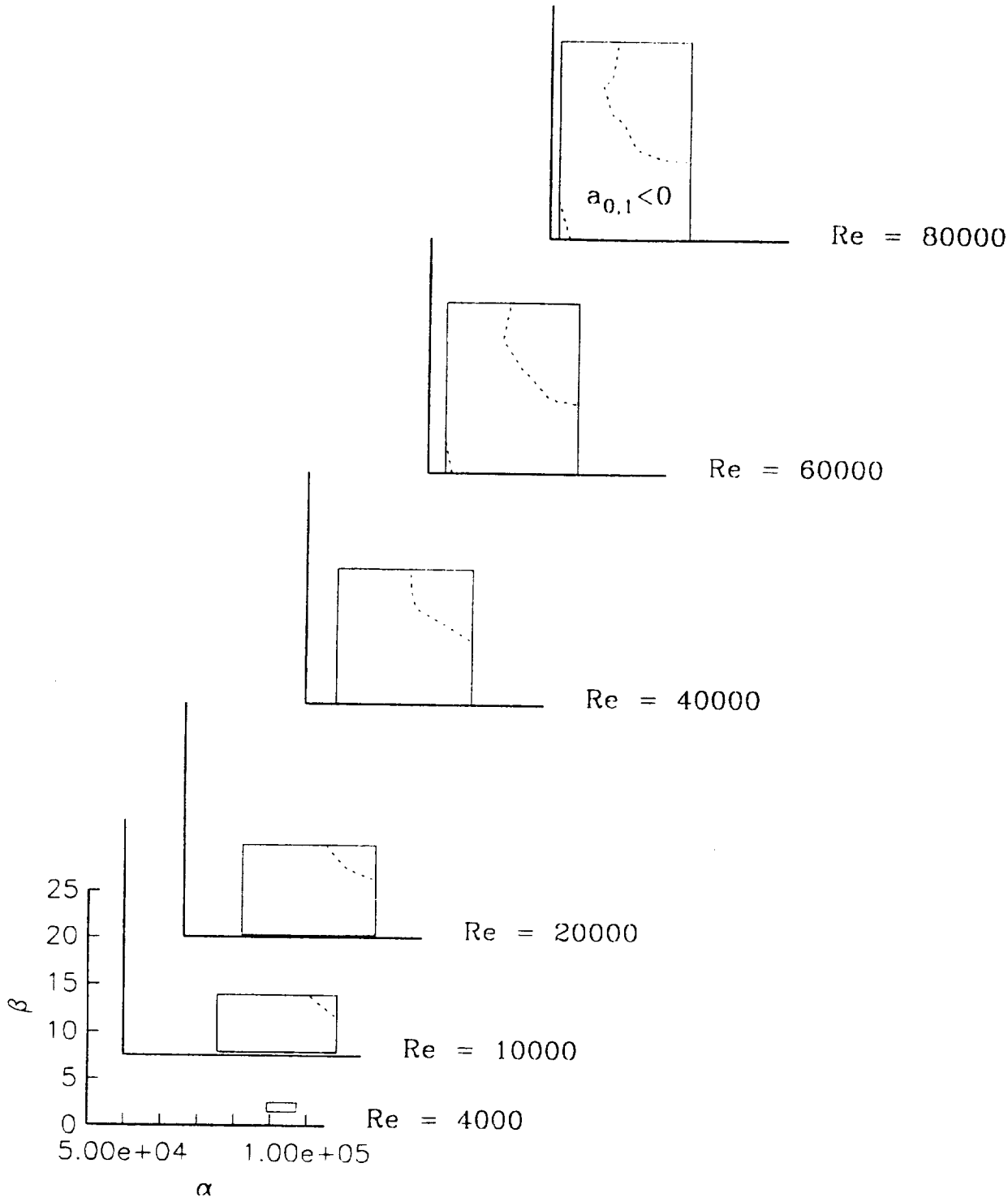

Figure 6: Zero contour of $a_{0,1}$, the effect of the Dean disturbance on the TS disturbance. The rectangles represent the range of α and β over which individual TS and Dean disturbances are linearly unstable at the given Reynolds number.

Figure 7

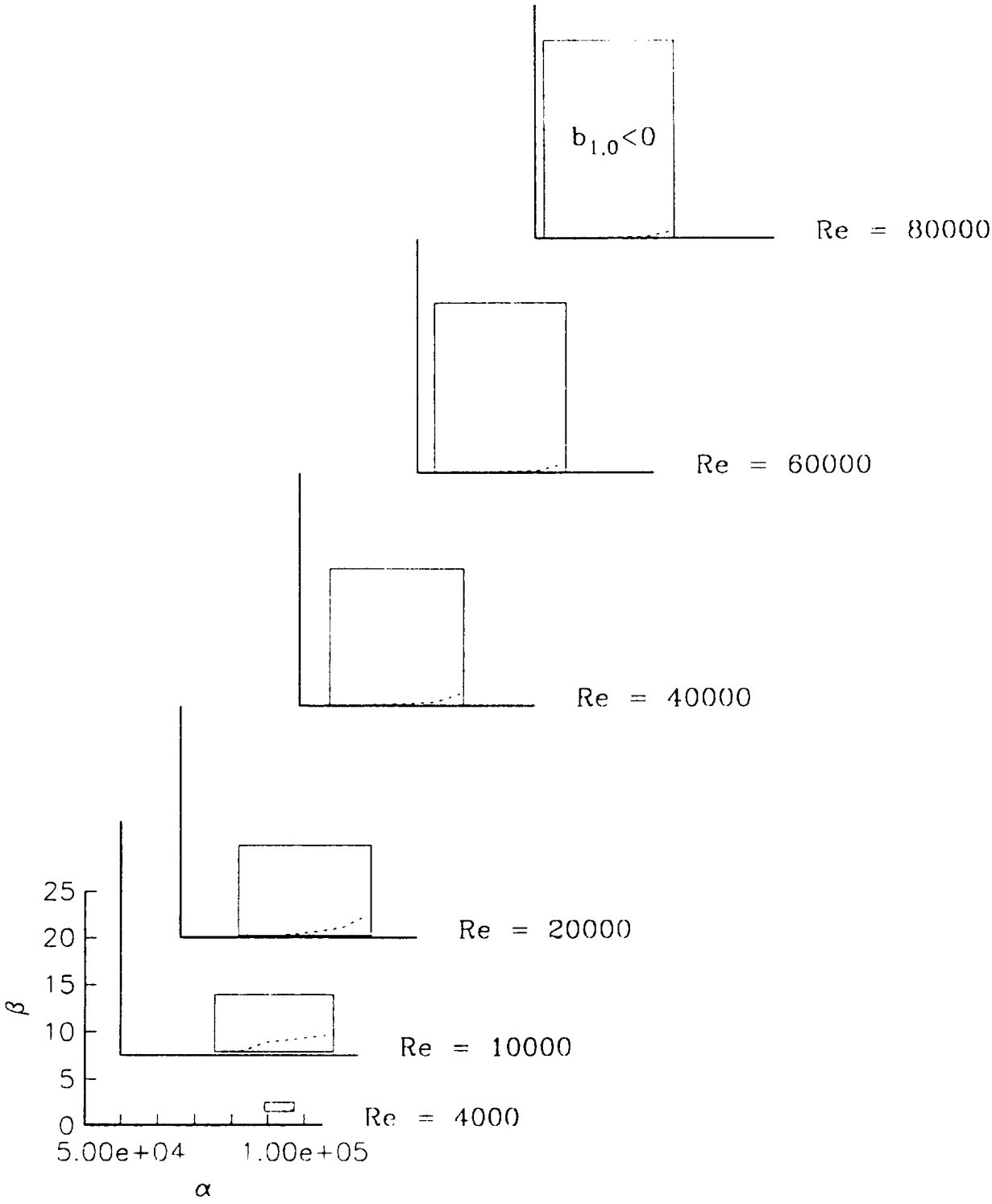

Figure 7: Zero contour of $b_{1,0}$, the effect of the TS disturbance on the Dean disturbance. The rectangles represent the range of α and β over which individual TS and Dean disturbances are linearly unstable at the given Reynolds number.

Figure 8

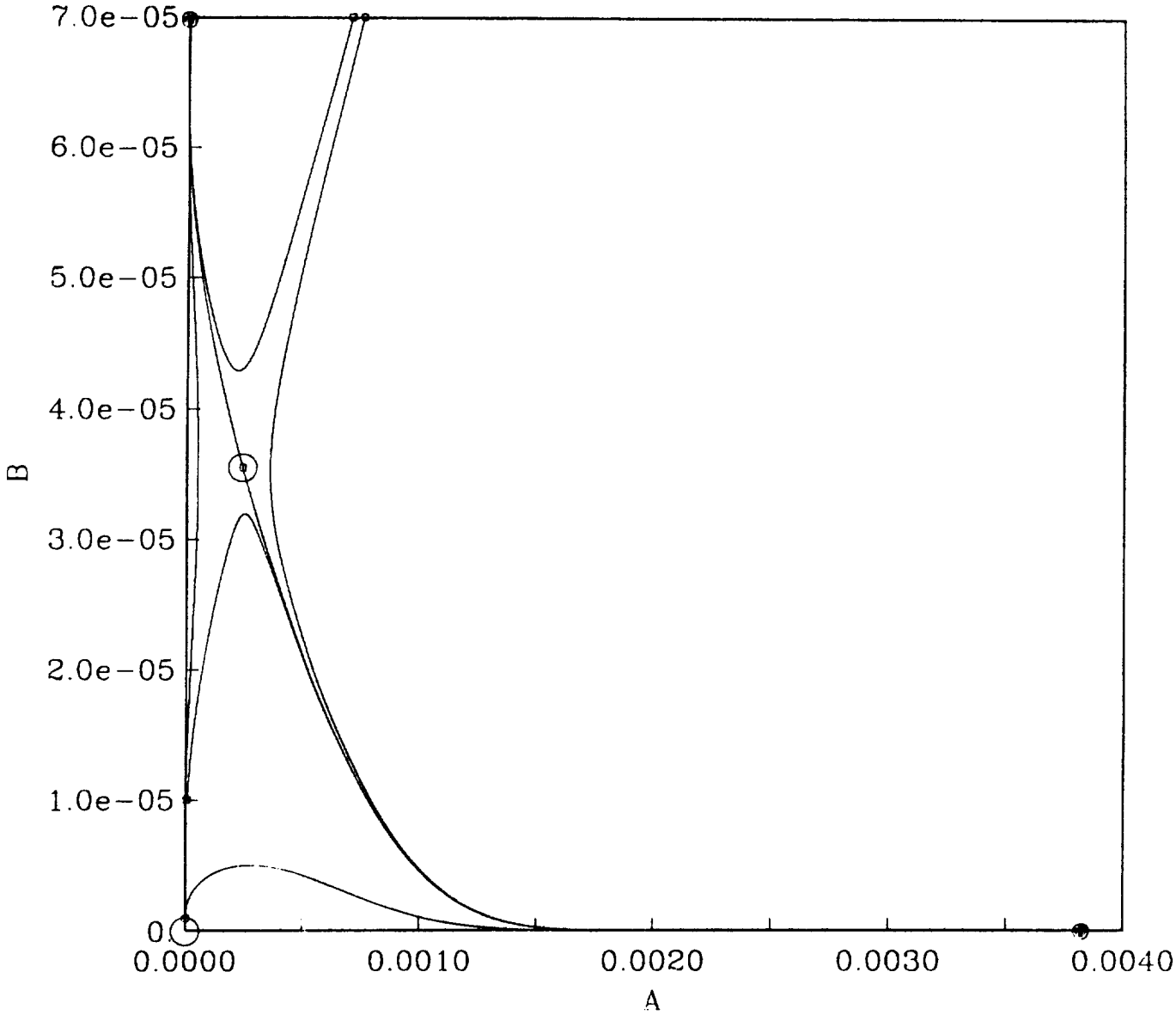

Figure 8: Trajectories in phase-space with Re = 6291.67, $\lambda = 2.189 \times 10^{-5}$, $\alpha = 74257$, and $\beta = 4.51$. Squares represent initial conditions, filled circles represent stable critical points. Open circles represent other critical points.

Figure 9

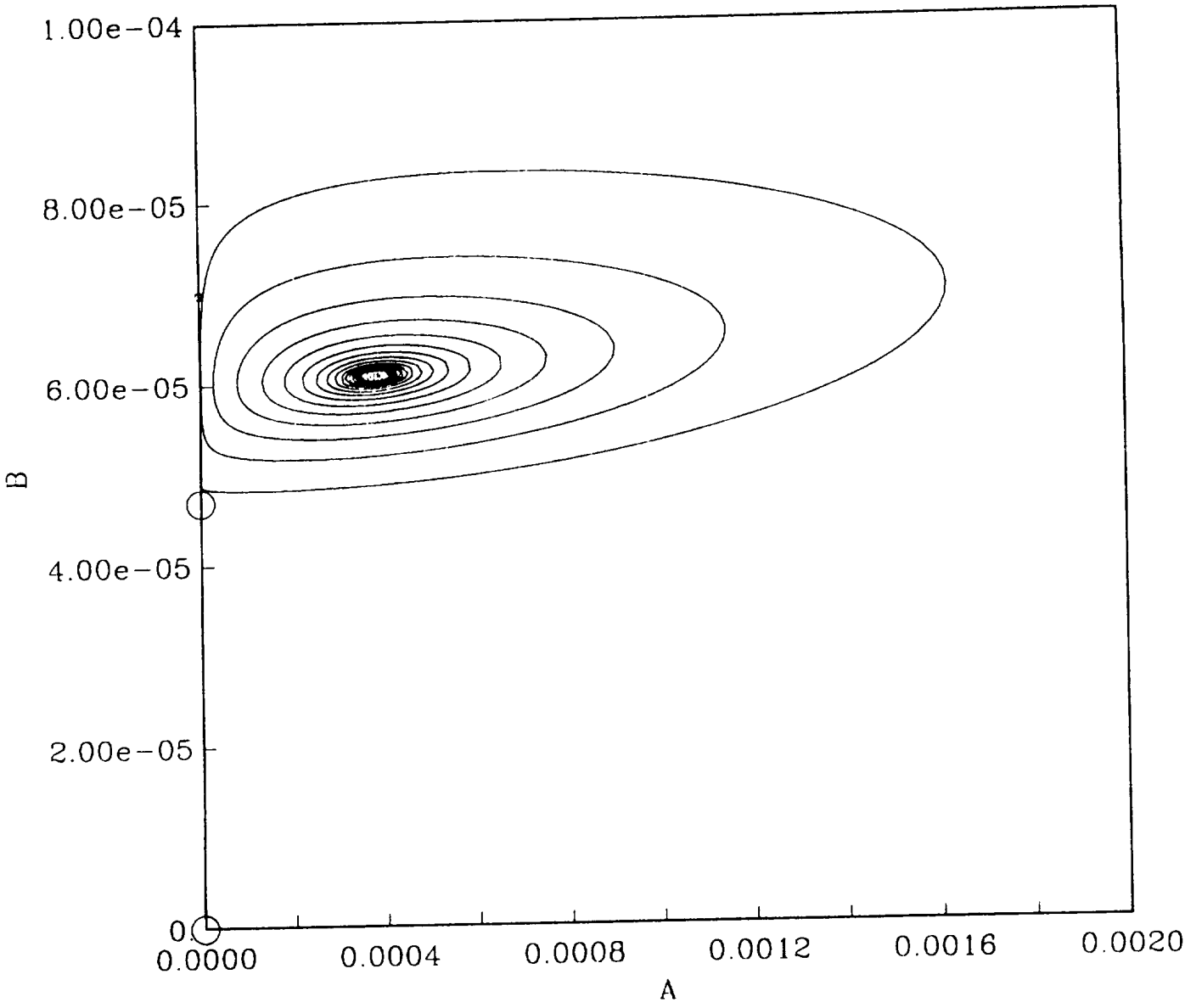

Figure 9: Trajectories in phase-space with Re = 4000, $\lambda = 2.179 \times 10^{-5}$, $\alpha = 96300$, and $\beta = 1.55$. Squares represent initial conditions, filled circles represent stable critical points. Open circles represent other critical points.

Figure 10

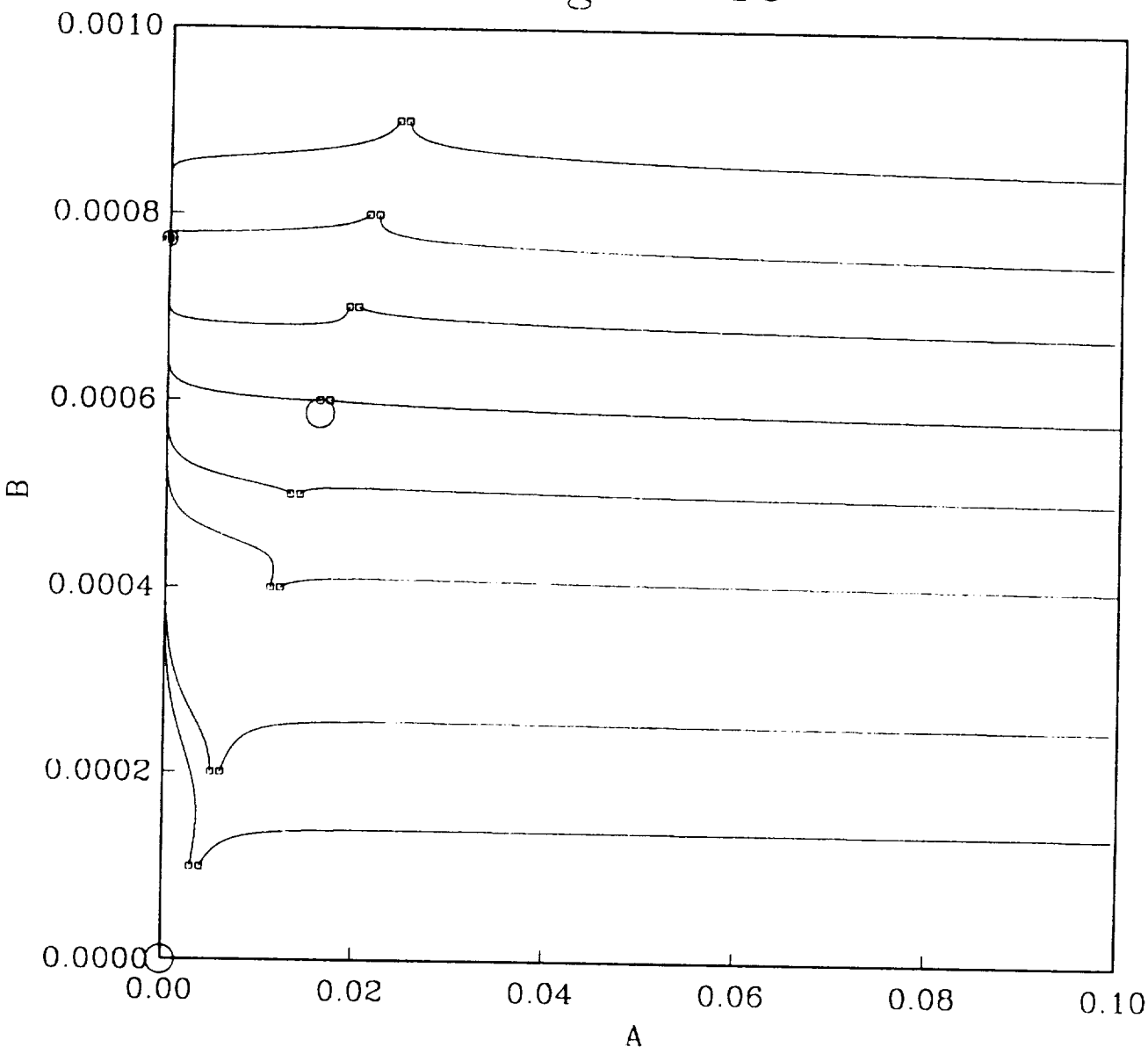

Figure 10: Trajectories in phase-space with Re = 5000, $\lambda = 2.179 \times 10^{-5}$, $\alpha = 100000$, and $\beta = 2.0$. Squares represent initial conditions, filled circles represent stable critical points. Open circles represent other critical points.

Figure 11

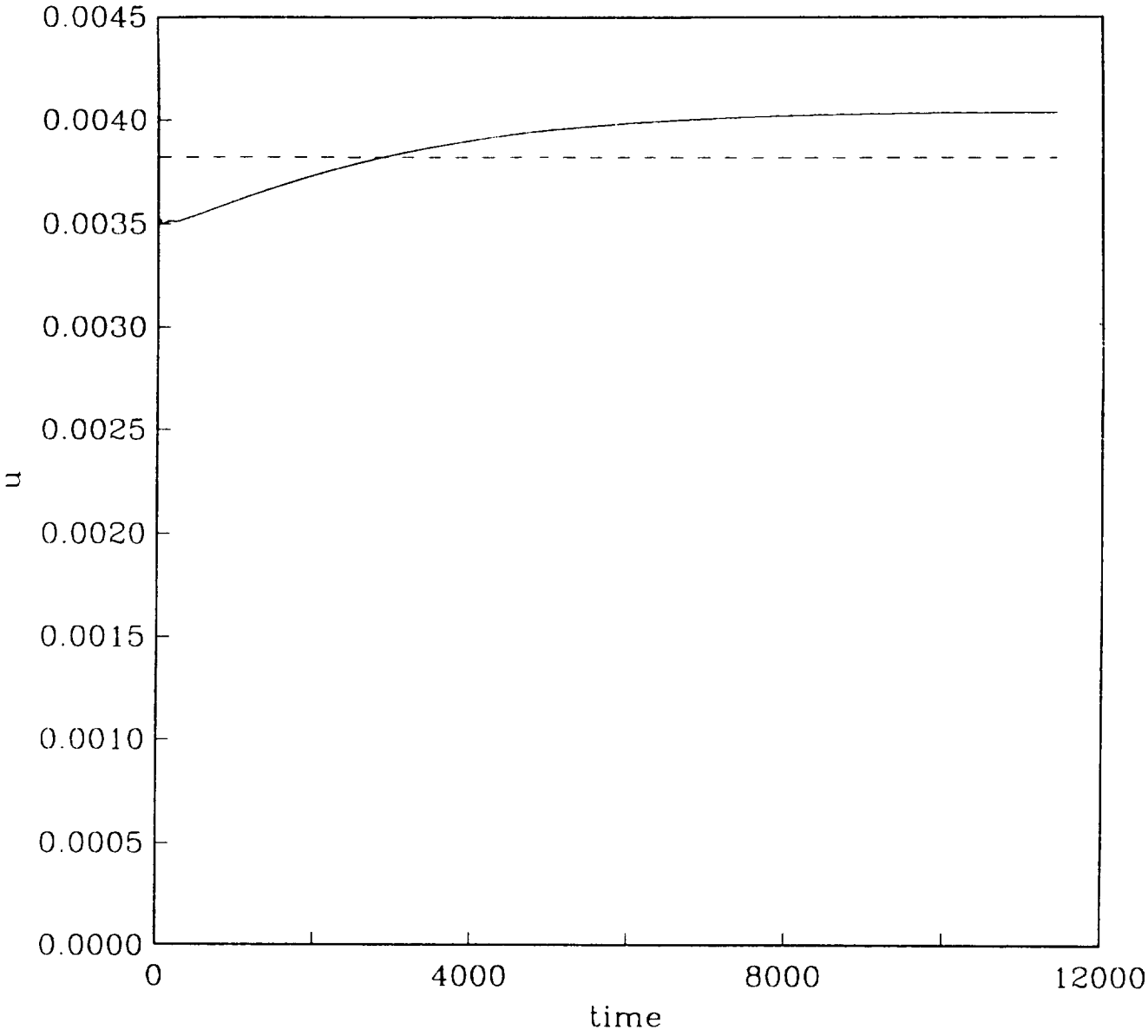

Figure 11: Amplitude evolution of TS wave (——). Weakly nonlinear theory equilibrium amplitude (----).

NASA SCIENTIFIC AND TECHNICAL DOCUMENT AVAILABILITY AUTHORIZATION (DAA)

To be initiated by the responsible NASA Project Officer, Technical Monitor, or other appropriate NASA official for all presentations, reports, papers, and proceedings that contain scientific and technical information. Explanations are on the back of this form and are presented in greater detail in NHB 2200.2, "NASA Scientific and Technical Information Handbook."

XX Original
☐ Modified

(Facility Use Only)
Control No. _____
Date _____

I. DOCUMENT/PROJECT IDENTIFICATION (Information contained on report documentation page should not be repeated except title, date and contract number)

Title: 15 - DEAN INTERACTIONS IN CURVED CHANNEL FLOW

Author(s): _____

Originating NASA Organization: Langley Research Center

Performing Organization (if different): Institute for Computer Applications in Science & Engineering (ICASE)*

Contract/Grant/Interagency/Project Number(s): NAS1-14097, NAS1-14101, NAS1-14472, NAS1-14927, NAS1-15810,**

Document Number(s): CR-181983 505-90-21-01 Document Date: _____

(For presentations or externally published documents, enter appropriate information on the intended publication such as name, place, and date of conference, periodical or journal title, or book title and publisher. _____

These documents must be routed to NASA Headquarters, International Affairs Division for approval. (See Section VII))

II. AVAILABILITY CATEGORY **NAS1-16394, NAS1-17070, NAS1-17130, NAS1-18107, NAS1-18605

Check the appropriate category(ies). NCC1-45

Security Classification: ☐ Secret ☐ Secret RD ☐ Confidential ☐ Confidential RD XX Unclassified

Export Controlled Document - Documents marked in this block must be routed to NASA Headquarters International Affairs Division for approval.

☐ ITAR ☐ EAR

NASA Restricted Distribution Document

☐ FEDD ☐ Limited Distribution ☐ Special Conditions-See Section III

Document disclosing an invention

☐ Documents marked in this block must be withheld from release until six months have elapsed after submission of this form, unless a different release date is established by the appropriate counsel. (See Section IX).

Publicly Available Document

XX Publicly available documents must be unclassified and may not be export-controlled or restricted distribution documents.

☐ Copyrighted ☐ Not copyrighted

*Operated by the Universities Space Research Association

IN-02
20671
450

III. SPECIAL CONDITIONS

Check one or more of the applicable boxes in each of (a) and (b) as the basis for special restricted distribution if the "Special Conditions" box under NASA Restricted Distribution Document in Section II is checked. Guidelines are provided on reverse side of form.

a. This document contains:

☐ Foreign government information ☐ Commercial product test or evaluation results ☐ Preliminary information ☐ Information subject to special contract provision

☐ Other – Specify _____

b. Check one of the following limitations as appropriate:

☐ U.S. Government agencies and U.S. Government agency contractors only ☐ NASA contractors and U.S. Government agencies only ☐ U.S. Government agencies only

☐ NASA personnel and NASA contractors only ☐ NASA personnel only ☐ Available only with approval of issuing office: _____

IV. BLANKET RELEASE (OPTIONAL)

All documents issued under the following contract/grant/project number (See above) may be processed as checked in Sections II and III.

The blanket release authorization granted 16 Aug. '89 (Date): effective through 30 Sept. 1990.

☐ Rescinded - Future documents must have individual availability authorizations. ☐ Modified - Limitations for all documents processed in the STI system under the blanket release should be changed to conform to blocks as checked in Section II.

V. PROJECT OFFICER/TECHNICAL MONITOR

Richard W. Barnwell (Typed Name of Project Officer/Technical Monitor) | MS 105A (Office Code) | Richard W Barnwell (Signature) | 6/16/89 (Date)

VI. PROGRAM OFFICE REVIEW ☒ Approved ☐ Not Approved

R. E. Rose (Typed Name of Program Office Representative) | RF (Program Office and Code) | R. E. Rose (Signature) | 8/16/89 (Date)

VII. INTERNATIONAL AFFAIRS DIVISION REVIEW

☐ Open, domestic conference presentation approved. ☐ Export controlled limitation is not applicable.

☐ Foreign publication/presentation approved. ☐ The following Export controlled limitation (ITAR/EAR) is assigned to this document: _____

☐ Export controlled limitation is approved.

_____ (International Affairs Div. Representative) _____ (Title) _____ (Date)

VIII. EXPIRATION OF REVIEW TIME

The document is being released in accordance with the availability category and limitation checked in Section II since no objection was received from the Program Office within 20 days of submission, as specified by NHB 2200.2, and approval by the International Affairs Division is not required.

Name & Title _____ Office Code _____ Date _____

Note: This release procedure cannot be used with documents designated as Export Controlled Documents, conference presentations or foreign publications.

IX. DOCUMENTS DISCLOSING AN INVENTION

a. This document may be released on _____ (Date) Installation Patent or Intellectual Property Counsel _____ Date _____

b. The document was processed on _____ (Date) in accordance with Sections II and III as applicable. NASA STI Facility _____ Date _____

X. DISPOSITION

Completed forms should be forwarded to the **NASA Scientific and Technical Information Facility, P.O. Box 8757, B.W.I. Airport, Maryland 21240**, with either (check box):

☐ Printed or reproducible copy of document enclosed

☐ Abstract or Report Documentation Page enclosed. The issuing or sponsoring NASA installation should provide a copy of the document, when complete, to the NASA Scientific and Technical Information Facility at the above listed address.